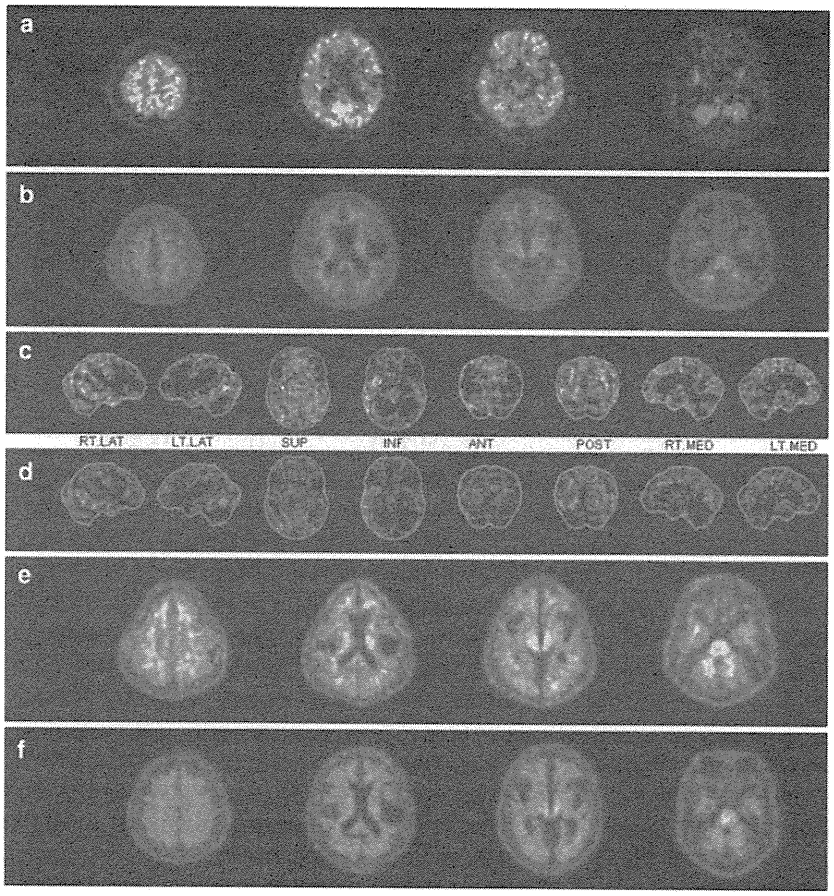

Fig. 1 An 81-year-old female with a diagnosis of MCI (MMSE was 26). **a** FDG PET did not demonstrate an AD pattern. **b** BF-227 PET did not demonstrate significantly increased uptake in the brain. **c** 3D-SSP results by Method 1 showed generalized significant abnormalities in the brain suggesting AD, although **d** those analyzed by Method 2 did not. This patient was followed up for 3 years, but did not convert to AD. **e** BF-227 images after co-registration to FDG images by Method 1. The distortions were seen mainly in the frontal lobes. **f** BF-227 images after co-registration to FDG images by Method 2. No distortions were seen

Table 2 The numbers of cases with distortions after Method 1

	AD	MCI	NC	Total
Slight	6	5	6	17
Strong	1	2	1	4
Total	7	7	7	21

A sample of anatomically standardized image with slight distortion.

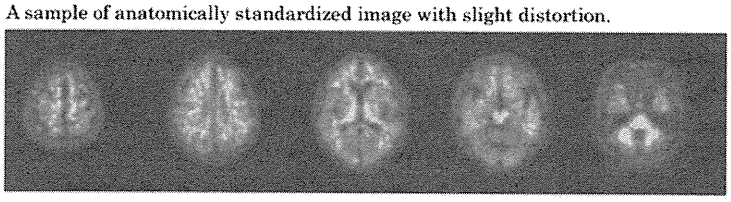

A sample of anatomically standardized image with strong distortion.

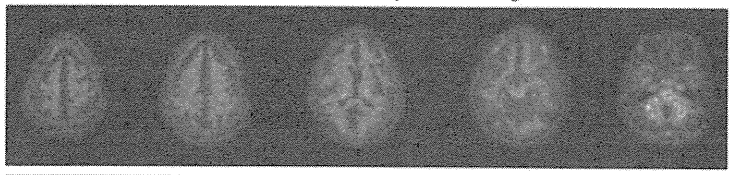

between MCI and NC in all the lobes, but Method 1 did not show a significant difference between MCI and NC in the frontal lobe (Fig. 2).

Method 2 demonstrated that converters showed significantly higher values than non-converters in the parietal and frontal lobes, which was not observed with Method 1 (Fig. 3).

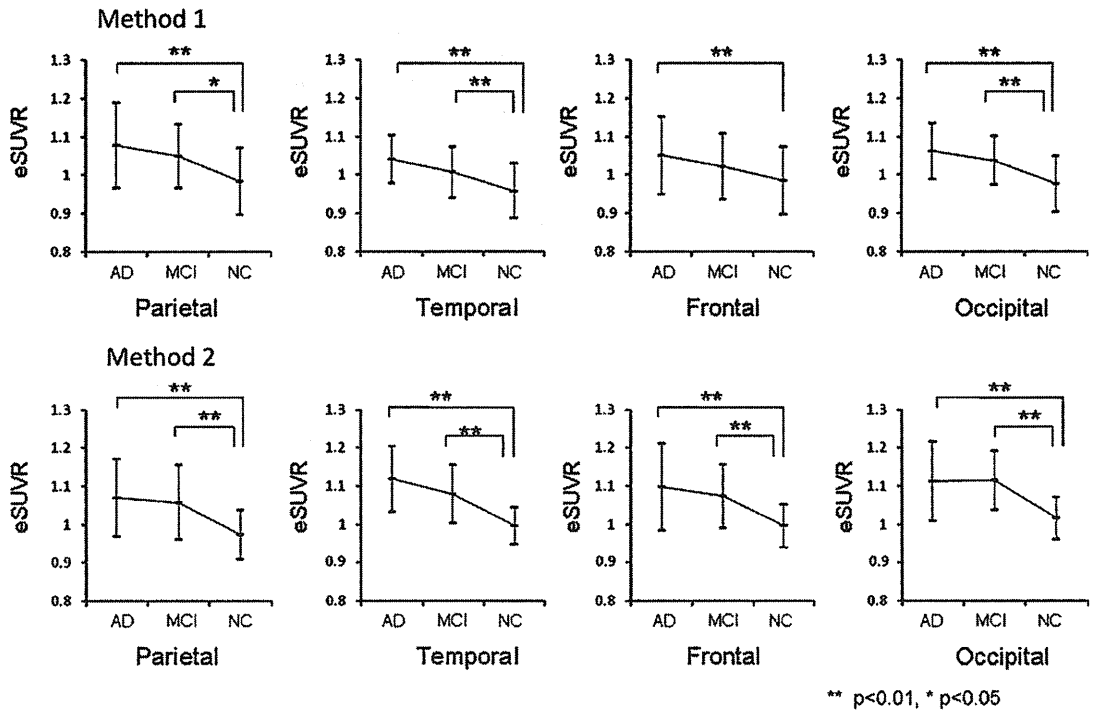

Fig. 2 Mean (SD) of eSUVR in the AD, MCI, and control groups calculated by Method 1 and 2. The values were calculated for the parietal, temporal, frontal, and occipital lobes

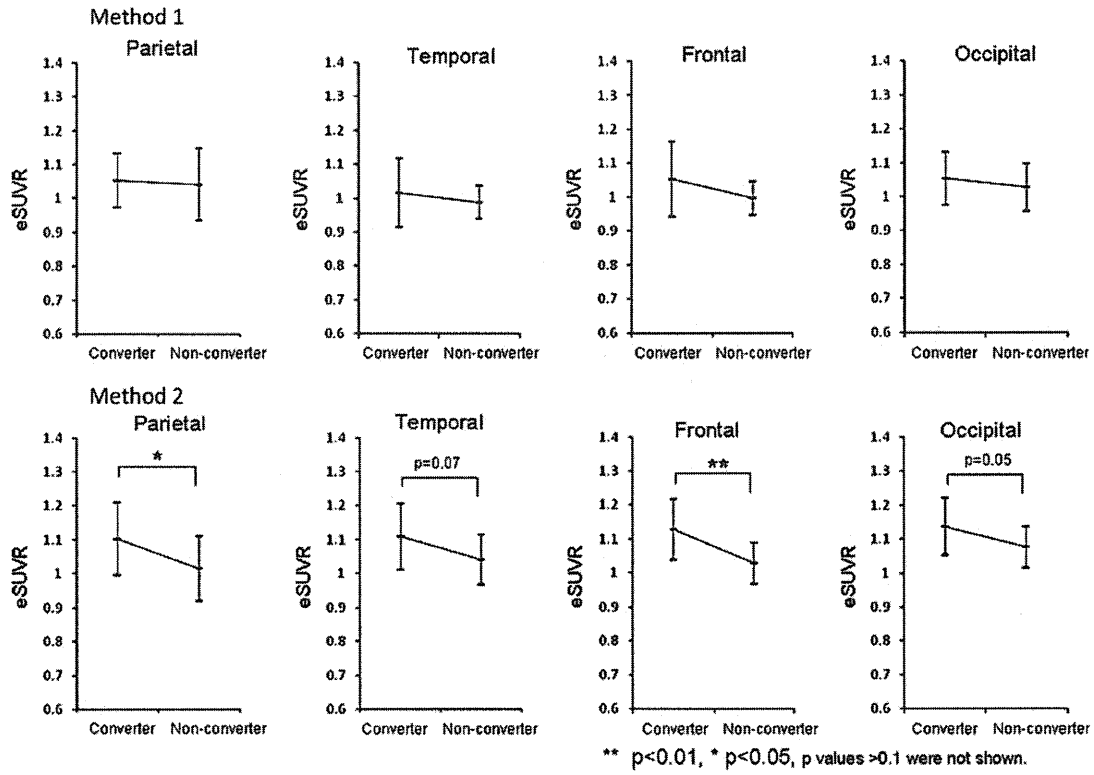

Fig. 3 Mean (SD) of eSUVR for MCI-to-AD converters and non-converters calculated by Method 1 and 2. The values were calculated for the parietal, temporal, frontal, and occipital lobes

3D-SSP analyses

Figure 4 a–c shows the *Z* score maps of 3D-SSP analyses processed by Method 1 and 2, comparing AD and NC, MCI and NC, and converters and non-converters. The differences between Method 1 and 2 were not clear in Fig. 4a, b; however, Fig. 4c demonstrated more intense and widespread abnormalities between converters and non-converters by Method 2 than by Method 1.

Figure 5 a–c shows the *Z* score maps processed by Method 2 comparing converters and NC, non-converters and NC, and converters and non-converters, respectively. Figure 5a reveals a similar distribution to that in Fig. 4a, b, but with the scores slightly higher than those in Fig. 4b and slightly lower than those in Fig. 4a. Figure 5b showed a globally low *z* score that was slightly higher in the left temporal lobe. Figure 5c demonstrated differences between converters and non-converters especially in both lateral frontal lobes.

Discussion

Voxel-based analysis allows an objective and sensitive identification of regional changes. Statistical parametric mapping (SPM) [7] and 3D-SSP have both been commonly used for voxel-based analysis for brain PET and SPECT. However, for amyloid PET analysis, most researchers have performed SPM analyses using an MR template after registration of PET images to MR images [8, 9]. In this case, the AS of SPM will not be influenced by the distribution of PET tracers. 3D-SSP can also utilize MR images, but this method is not commonly performed. The 3D-SSP analysis of amyloid PET images using an FDG template entails the problems mentioned in "Introduction". In fact, our results demonstrated that Method 1 showed varying degrees of errors for AS in 38% of the cases. These errors may not only produce an overestimation or underestimation of the amyloid burden in the brain, but also result in the creation of inaccurate normal databases for voxel-based analysis. Thus, Method 1 seems inappropriate for 3D-SSP analysis of amyloid PET. FDG PET has been widely accepted as the method to assess functional abnormalities in dementia [10–12], and is commonly used for clinical evaluation of patients with MCI and AD. Most of those who underwent amyloid PET have also undergone FDG PET. We proposed to take advantage of this coupling of PET images to solve the problem of 3D-SSP analysis for amyloid PET. Although this problem has been noticed by some researchers, to our knowledge, this is the first paper to demonstrate this problem and present a solution.

For AS of the brain images, a standard stereotactic atlas brain (template) is necessary. Although templates differ to some degree between software programs, a template is basically created by averaging a large number of normal scans. In addition, Neurostat uses hundreds of predefined landmarks for nonlinear warping [1]. It seemed difficult to create an original template with landmarks for amyloid PET by ourselves. Therefore, the next step was to utilize an FDG template after co-registration of FDG and BF-227 images. Because these images are obtained from the same subjects, it is possible to register them accurately using linear transformation methods, such as translocations and rotations. For the registration criterion, Neurostat uses mutual information (MI). The MI of the image intensity values of corresponding voxel pairs is maximal if the images are geometrically aligned. Because no assumptions are made regarding the nature of the relation between the image intensities in both modalities, this criterion is very general and powerful and can be applied automatically without prior segmentation to a large variety of techniques [13–16]. After the registration, Neurostat successfully warped registered BF-227 images using transformation parameters calculated for the AS of corresponding FDG images.

Results of regional analysis demonstrated that both Method 1 and 2 showed significantly higher uptake in AD and MCI patients compared to NC subjects for most lobes, but Method 1 did not show significant differences between MCI and NC subjects for the frontal lobe. In addition, only Method 2 demonstrated significant differences between converters and non-converters. These differences were also obvious on 3D-SSP results when Method 2 was used. Because BF-227 is thought to have lower sensitivity for diffuse amyloid plaques, and a higher sensitivity for neuritic plaques than PiB, BF-227 has been reported to have potential as a method for predicting the conversion from MCI to AD accurately [6, 17, 18]. Previous regions-of-interest analyses for almost same subjects with this study demonstrated that increased BF-227 retention was evident in both the converters and AD patients, but not in the control subjects or the non-converters [17]. Considering these facts, Method 2 seems to provide more sensitive and accurate results than Method 1. In addition, 3D-SSP results subjected to Method 2 showed preferential accumulation in the temporal lobes, supporting previous reports that used SPM [19].

The new method, however, has some limitations. First, it requires successful FDG scans. If an FDG image has problems, Method 2 cannot be applied to it. Another problem with Method 2 is the possible creation of errors by misregistration of amyloid images. While the reason for this is not clear, it has been reported that standardization by 3D-SSP was not accurate enough at a head tilt of approximately 25° or more [20]. It is thus important to check each image after registration and AS.

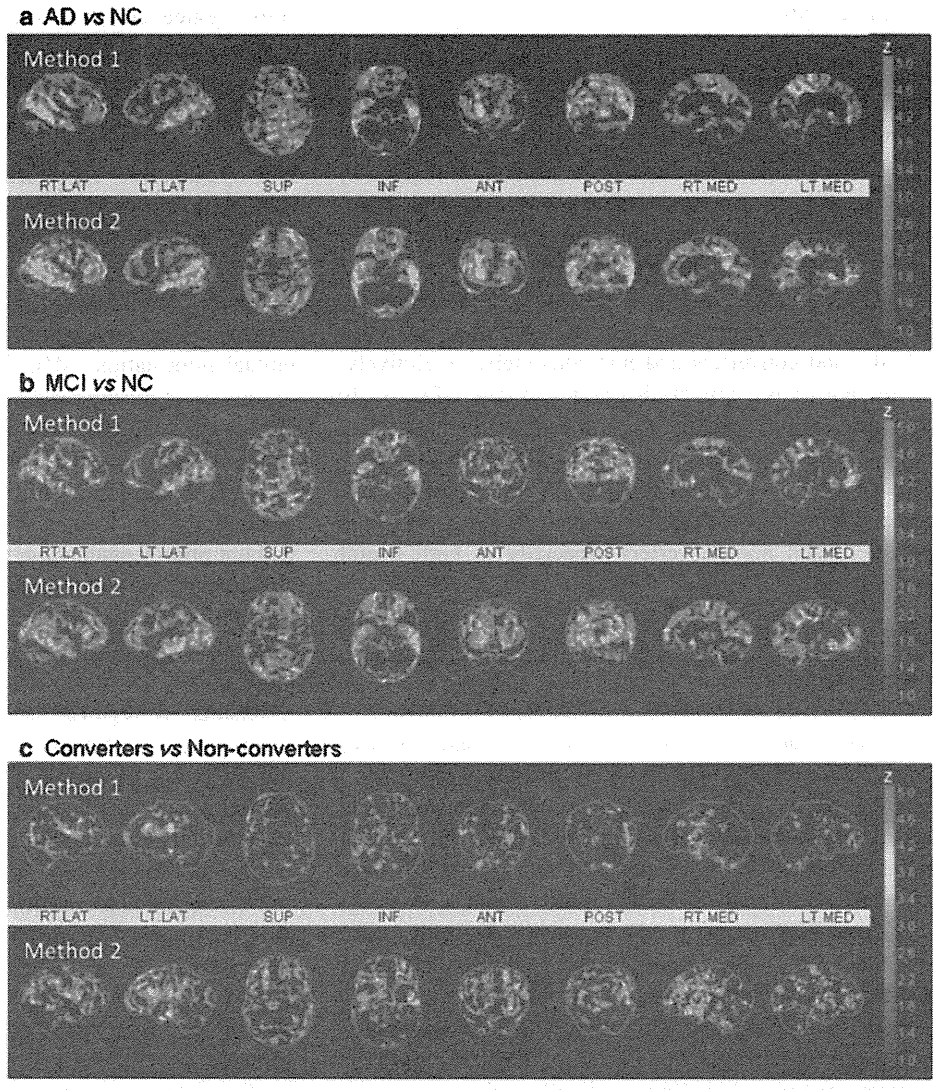

Fig. 4 *Z* score maps of 3D-SSP analyses processed by Method 1 and 2 of the **a** AD group compared to NC group, the **b** MCI group compared to NC group, and **c** converters compared to non-converters

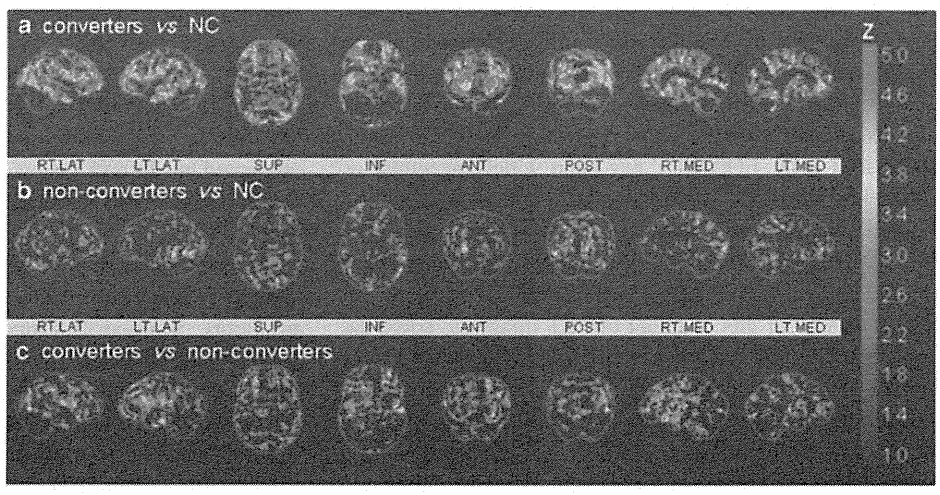

Fig. 5 *Z* score maps processed by Method 2 of **a** converters compared to NC group, **b** non-converters compared to NC group, and **c** converters compared to non-converters

We would like to conclude that our newly developed method can be used to modify errors in 3D-SSP analyses of amyloid PET imaging. 3D-SSP analysis of BF-227 PET was useful for detecting differences between AD and NC groups, MCI and NC groups, and converters and non-converters. Further investigation is required for the evaluation of the utility for individual differentiations.

Acknowledgments We appreciate the technical assistance provided by Seiichi Watanuki of CYRIC in Tohoku University (Sendai, Japan) and Frank Thiele of Philips Research North America (NY, USA).

Sources of funding for the article None.

References

1. Minoshima S, Koeppe RA, Frey KA, Kuhl DE. Anatomic standardization: linear scaling and nonlinear warping of functional brain images. J Nucl Med. 1994;35:1528–37.
2. Minoshima S, Frey KA, Koeppe RA, Foster NL, Kuhl DE. A diagnostic approach in Alzheimer's disease using three-dimensional stereotactic surface projections of fluorine-18-FDG PET. J Nucl Med. 1995;36:1238–48.
3. Klunk WE, Engler H, Nordberg A, Wang Y, Blomqvist G, Holt DP, et al. Imaging brain amyloid in Alzheimer's disease with Pittsburgh Compound-B. Ann Neurol. 2004;55:306–19.
4. Nordberg A. PET imaging of amyloid in Alzheimer's disease. Lancet Neurol. 2004;3:519–27.
5. Kudo Y. Development of amyloid imaging PET probes for an early diagnosis of Alzheimer's disease. Minim Invasive Ther Allied Technol. 2006;15:209–13.
6. Kudo Y, Okamura N, Furumoto S, Tashiro M, Furukawa K, Maruyama M, et al. 2-(2-[2-Dimethylaminothiazol-5-yl]ethenyl)-6-(2-[fluoro]ethoxy)benzoxazole: a novel PET agent for in vivo detection of dense amyloid plaques in Alzheimer's disease patients. J Nucl Med. 2007;48:553–61.
7. Friston KJ, Holmes AP, Worsley KJ, Poline JB, Frith C, Frackowiak RSJ. Statistical parametric maps in functional imaging: a general linear approach. Hum Brain Mapp. 1995;2:189–210.
8. Mikhno A, Devanand D, Pelton G, Cuasay K, Gunn R, Upton N, et al. Voxel-based analysis of 11C-PIB scans for diagnosing Alzheimer's disease. J Nucl Med. 2008;49:1262–9.
9. Ziolko SK, Weissfeld LA, Klunk WE, Mathis CA, Hoge JA, Lopresti BJ, et al. Evaluation of voxel-based methods for the statistical analysis of PIB PET amyloid imaging studies in Alzheimer's disease. Neuroimage. 2006;33:94–102.
10. de Leon MJ, Convit A, Wolf OT, Tarshish CY, DeSanti S, Rusinek H, et al. Prediction of cognitive decline in normal elderly subjects with 2-[(18)F]fluoro-2-deoxy-D-glucose/positron-emission tomography (FDG/PET). Proc Natl Acad Sci. 2001;98:10966–71.
11. Minoshima S, Giordani B, Berent S, Frey KA, Foster NL, Kuhl DE. Metabolic reduction in the posterior cingulate cortex in very early Alzheimer's disease. Ann Neurol. 1997;42:85–94.
12. Mosconi L, De Santi S, Li Y, Li J, Zhan J, Tsui WH, et al. Visual rating of medial temporal lobe metabolism in mild cognitive impairment and Alzheimer's disease using FDG-PET. Eur J Nucl Med Mol Imaging. 2006;33:210–21.
13. Maes F, Collignon A, Vandermeulen D, Marchal G, Suetens P. Multimodality image registration by maximization of mutual information. IEEE Trans Med Imaging. 1997;16:187–98.
14. Maes F, Vandermeulen D, Suetens P. Comparative evaluation of multiresolution optimization strategies for multimodality image registration by maximization of mutual information. Med Image Anal. 1999;3:373–86.
15. Pluim JP, Maintz JB, Viergever MA. Image registration by maximization of combined mutual information and gradient information. IEEE Trans Med Imaging. 2000;19:809–14.
16. Pluim JP, Maintz JB, Viergever MA. Mutual-information-based registration of medical images: a survey. IEEE Trans Med Imaging. 2003;22:986–1004.
17. Waragai M, Okamura N, Furukawa K, Tashiro M, Furumoto S, Funaki Y, et al. Comparison study of amyloid PET and voxel-based morphometry analysis in mild cognitive impairment and Alzheimer's disease. J Neurol Sci. 2009;285:100–8.
18. Furukawa K, Okamura N, Tashiro M, Waragai M, Furumoto S, Iwata R, et al. Amyloid PET in mild cognitive impairment and Alzheimer's disease with BF-227: comparison to FDG-PET. J Neurol. 2010;257:721–7.
19. Shao H, Okamura N, Sugi K, Furumoto S, Furukawa K, Tashiro M, et al. Voxel-based analysis of amyloid positron emission tomography probe [C]BF-227 uptake in mild cognitive impairment and alzheimer's disease. Dement Geriatr Cogn Disord. 2010;30:101–11.
20. Onishi H, Matsutake Y, Kawashima H, Matsutomo N, Amijima H. Comparative study of anatomical normalization errors in SPM and 3D-SSP using digital brain phantom. Ann Nucl Med. 2011;25:59–67.

Eur J Nucl Med Mol Imaging (2011) 38:343–351
DOI 10.1007/s00259-010-1612-0

ORIGINAL ARTICLE

In vivo changes in microglial activation and amyloid deposits in brain regions with hypometabolism in Alzheimer's disease

Masamichi Yokokura · Norio Mori · Shunsuke Yagi · Etsuji Yoshikawa · Mitsuru Kikuchi · Yujiro Yoshihara · Tomoyasu Wakuda · Genichi Sugihara · Kiyokazu Takebayashi · Shiro Suda · Yasuhide Iwata · Takatoshi Ueki · Kenji J. Tsuchiya · Katsuaki Suzuki · Kazuhiko Nakamura · Yasuomi Ouchi

Received: 29 May 2010 / Accepted: 25 August 2010 / Published online: 16 September 2010

Abstract
Purpose Amyloid β protein (Aβ) is known as a pathological substance in Alzheimer's disease (AD) and is assumed to coexist with a degree of activated microglia in the brain. However, it remains unclear whether these two events occur in parallel with characteristic hypometabolism in AD in vivo. The purpose of the present study was to clarify the in vivo relationship between Aβ accumulation and neuroinflammation in those specific brain regions in early AD.
Methods Eleven nootropic drug-naïve AD patients underwent a series of positron emission tomography (PET) measurements with [^{11}C](*R*)PK11195, [^{11}C]PIB and [^{18}F]FDG and a battery of cognitive tests within the same day. The binding potentials (BPs) of [^{11}C](*R*)PK11195 were directly compared with those of [^{11}C]PIB in the brain regions with reduced glucose metabolism.
Results BPs of [^{11}C](*R*)PK11195 and [^{11}C]PIB were significantly higher in the parietotemporal regions of AD patients than in ten healthy controls. In AD patients, there was a negative correlation between dementia score and [^{11}C](*R*)PK11195 BPs, but not [^{11}C]PIB, in the limbic, precuneus and prefrontal regions. Direct comparisons showed a significant negative correlation between [^{11}C](*R*)PK11195 and [^{11}C]PIB BPs in the posterior cingulate cortex (PCC) ($p<0.05$, corrected) that manifested the most severe reduction in [^{18}F]FDG uptake.
Conclusion A lack of coupling between microglial activation and amyloid deposits may indicate that Aβ accumulation shown by [^{11}C]PIB is not always the primary cause of microglial activation, but rather the negative correlation present in the PCC suggests that microglia can show higher activation during the production of Aβ in early AD.

Electronic supplementary material The online version of this article (doi:10.1007/s00259-010-1612-0) contains supplementary material, which is available to authorized users.

M. Yokokura · N. Mori · Y. Yoshihara · T. Wakuda · K. Takebayashi · Y. Iwata · K. Nakamura
Department of Psychiatry and Neurology,
Hamamatsu University School of Medicine,
Hamamatsu, Japan

S. Yagi · Y. Ouchi (✉)
Laboratory of Human Imaging Research,
Molecular Imaging Frontier Research Center,
Hamamatsu University School of Medicine,
1-20-1 Handayama, Higashi-ku,
Hamamatsu 431-3192, Japan
e-mail: ouchi@hama-med.ac.jp

E. Yoshikawa
Central Research Laboratory, Hamamatsu Photonics K.K.,
Hamamatsu, Japan

M. Kikuchi
Department of Psychiatry and Neurobiology,
Graduate School of Medical Science, Kanazawa University,
Kanazawa, Japan

G. Sugihara · S. Suda · K. J. Tsuchiya · K. Suzuki
Research Center for Child Mental Development,
Hamamatsu University School of Medicine,
Hamamatsu, Japan

T. Ueki
Department of Anatomy,
Hamamatsu University School of Medicine,
Hamamatsu, Japan

Keywords Alzheimer's disease · Microglia · Amyloid β protein · Positron emission tomography

Introduction

Amyloid β protein (Aβ) accumulation is important in the pathology of Alzheimer's disease (AD). The amyloid hypothesis here posits that Aβ accumulation is responsible for triggering tau phosphorylation and neurofibrillary tangle formation, which lead to neurodegeneration in AD [1]. It has been reported that Aβ accumulation can activate microglia [2–4], and the activated microglia in turn accelerate Aβ accumulation by releasing proinflammatory neurotoxic substances [5–7]. In the AD brain, the region of increased microglial activity likely accompanies cerebral glucose hypometabolism and a higher rate of brain atrophy, suggesting that the degree of microglial activation predicts disease progression in AD [8].

Aβ accumulation would reportedly precede a decline in glucose metabolism and cognitive function and reach a plateau at an early clinical stage of AD [9, 10]. However, the Aβ accumulation seems unrelated to the reductions in glucose metabolism or Mini-Mental State Examination (MMSE) scores in AD patients [10–14]. In contrast to the fibril form of Aβ, soluble Aβ oligomer that is produced earlier than formation of Aβ fibrils is considered to be a more deleterious substance which can activate microglia and stimulate secretion of cytokines [2–4]. Although animal experiments hinted that microglial activity could increase before Aβ accumulation [15, 16], little is known about the relationship between activated microglia and Aβ oligomer or fibril accumulation in the AD brain in vivo.

To clarify the in vivo relationships among these events, i.e. microglia activation, Aβ accumulation and glucose metabolism or neuronal function, we for the first time measured the levels of binding of radiotracers that could reflect those severities in early AD within the same day by PET.

Materials and methods

Participants

A total of 15 patients were initially enrolled in this study, but 4 patients were unable to proceed to the third PET measurement (glucose metabolism) because they unintentionally had a meal before the third scan. Accordingly, we collected data from 11 patients with AD (6 men and 5 women; mean age 70.6±6.4 years) who were all able to undergo three kinds of PET scans in this study. The diagnosis of AD was based on the criteria of the National Institute of Neurological and Communicative Disorders and Stroke-Alzheimer's Disease and Related Disorders Association (NINCDS/ADRDA) [17] and the Diagnostic and Statistical Manual of Mental Disorders-IV (DSM-IV). The exclusion criteria were: (1) the presence of significant white matter microvascular changes on magnetic resonance imaging (MRI) over and above a few scattered lacunes compatible with normal aging, (2) smoking and drinking much alcohol regularly, (3) taking donepezil, antipsychotics and hypnotics, (4) taking anxiolytics and nonsteroidal anti-inflammatory drugs (NSAIDs) regularly and (5) having untreated hypertension or diabetes. The above exclusion criteria were also applied when selecting age-matched healthy control subjects (n=10 for [^{11}C](*R*)PK11195 measurement, n=11 for [^{11}C]PIB and [^{18}F]FDG measurements). Neuropsychological assessment for all AD patients comprised a MMSE, word generation test and cubic copy as shown in Table 1. Healthy controls had no neurological problems and no abnormalities on MRI. The present study was approved by the Ethics Committee of the Hamamatsu Medical Center, and written informed consent was obtained from all participants.

MRI scanning

MRI was performed to determine the areas of the regions to be used for setting regions of interest (ROIs) using a static magnet (0.3 T MRP7000AD, Hitachi, Tokyo, Japan) with the following acquisition parameters; three-dimensional mode sampling, repetition time (TR)/echo time (TE) (200/23), 75° flip angle, 2-mm slice thickness with no gap and 256×256 matrices. The MRI measures and a mobile PET gantry allowed us to reconstruct the PET images parallel to the intercommissural (ACPC) line without reslicing; using this approach, we were able to allocate ROIs on the target regions of the original PET images [18].

PET data acquisition

Patients underwent a series of PET measurements after a battery of neuropsychological tests and MRI. We used a high-resolution brain PET scanner (SHR12000, Hamamatsu Photonics K.K., Hamamatsu, Japan), which was capable of yielding 47 tomographic images [19]. A 10-min transmission scan for attenuation correction using a ^{68}Ge/^{68}Ga source was conducted with the subject's head fixed by a radiosurgery-purpose thermoplastic face mask under resting conditions. After backprojection and filtering (Hanning filter, cutoff frequency 0.2 cycles per pixel), the image resolution was 2.9×2.9×3.4 mm full-width at half-maximum (FWHM). The voxel of each reconstructed image measured 1.3×1.3×3.4 mm. After a bolus intravenous injection of 280 MBq dose of [^{11}C](*R*)PK11195, 32

Table 1 Characteristics of AD patients

Patient No.	Age	Sex	Handedness	Disease duration[a]	MMSE	Word generation[b]		Cubic copy[c]
(n=11)	(years)			(years)		Correct	Incorrect	
1	70	F	Right	7	18	7	5	×
2	69	M	Right	3	16	2	0	×
3	76	M	Rght	3	24	7	0	○
4	69	F	Right	1	23	9	4	○
5	69	F	Right	2	20	6	2	×
6	81	M	Right	0.5	25	11	4	○
7	74	F	Right	2	22	4	0	○
8	57	M	Right	1	25	12	0	○
9	75	M	Right	2	26	10	0	○
10	75	M	Right	3	15	3	0	×
11	62	F	Right	2	23	8	3	○
Mean ± SD	70.6±6.4			2.4±1.7	21.5±3.5			

[a] The duration between disease onset and PET examination

[b] Word generation test: counting as many words as possible within 1 min from a category of animals. In this table, the word "correct" means the number of words from an appropriate category and "incorrect" means an inappropriate one

[c] Cubic copy: ○ correct, × incorrect

serial PET scans (time frames: 4×30, 20×60 and 8×300 s) were performed within 62 min. After taking a rest for 2.5 h, 40 serial PET scans (time frames: 12×10, 18×60 and 10×300 s) were performed during 70 min after injection of 280 MBq [^{11}C]PIB. Later, a static 15-min PET scan was done 45 min after injection of 100 MBq dose of [^{18}F]FDG. No arterial sampling was performed in each measurement.

Image data processing

The binding potential (BP) of [^{11}C](*R*)PK11195 was estimated based on a simplified reference tissue model [20, 21], in which we used a normalized mean time-activity curve created from control subjects as a reference tissue curve. This procedure has been described elsewhere [22]. Briefly, a normalized input curve was first created by averaging the ROIs placed over the bilateral frontal cortex, temporal cortex, thalamus, basal ganglia, cerebellar hemisphere and brain stem in the control group. The normalized mean tissue-activity curve was then used as the reference input function, because the desirable reference region free from specific binding is not present in patients with neurodegenerative disorders. The normalized input curve derived from the control group was used as the time-activity curve for the reference region of both the control subjects and AD patients.

To evaluate Aβ accumulation, [^{11}C]PIB BP was estimated based on a noninvasive Logan plot method using an input curve created from the cerebellar hemisphere in each subject [23, 24]. All BP parametric PET images were generated using PMOD 2.95 software (PMOD Technologies Ltd., Zurich, Switzerland).

To evaluate neuronal function (glucose metabolism), a semi-quantitative ratio index of [^{18}F]FDG was calculated as standardized uptake value ratio (SUVR), where the SUV showed tracer activity per injected dose normalized to body weight and then the SUVs of each region in the AD subjects were divided by the SUV of the cerebellar hemisphere in the same subjects and expressed as the SUVRs.

Image data analysis and statistics

SPM analysis

To explore the brain regions showing characteristic accumulation of the radiotracers, we examined the whole brain using a voxel-wise analytic method. For this purpose, SPM2 was used (Wellcome Department of Cognitive Neurology, London, UK, http://www.fil.ion.ucl.ac.uk/spm/software/spm2/). All [^{11}C](*R*)PK11195 BP, [^{11}C]PIB BP and [^{18}F]FDG SUVR parametric images were first normalized to the Montreal Neurological Institute space and smoothed with an isotropic Gaussian kernel of 8 mm. The between-group comparisons (AD vs healthy control) for each parameter were performed using t statistics on a voxel-by-voxel basis with a statistical threshold set at $p<0.05$ corrected for multiple comparisons (FDR), where the MMSE scores served as confounding covariates.

ROI analysis

Referring to the knowledge from the results of SPM analysis, multiple ROIs (44–474 mm^2) were drawn bilaterally over the anterior cingulate cortex (ACC), posterior cingulate cortex (PCC), precuneus (Prec), superior frontal cortex (SFC) (Brodmann area or BA9), middle frontal cortex (MFC) (BA9), parahippocampal cortex (PHC) and hippocampus (Hip) on the ACPC-aligned MR images of each subject [25]. Using an image processing system (Dr. View, Asahi Kasei Co., Tokyo, Japan), we determined ROIs on the MR images reformatted to the size of PET images. While PET images were displayed side by side together with the MR images, the delineated ROIs were placed on the same area on both the MR and the corresponding PET images. Because both reconstructed PET and MRI images were obtained parallel to the intercommissural line, they theoretically required no reorientation procedure [26]. In this way, these ROIs were transferred onto the corresponding quantitative PET parametric images. We examined correlations between MMSE scores and PET parameters in each delineated brain region. We also made direct comparisons among PET parameters obtained across multiple ROIs. The Pearson correlation and simple regression analyses were used with statistical significance set at $p<0.05$ corrected for multiple comparisons (SPSS version 17 J; SPSS Japan Inc., Tokyo, Japan).

Results

Levels of each PET parameter in AD patients vs healthy controls

The SPM analysis showed significant increases in [^{11}C](*R*)PK11195 BP in the medial frontal and parietal cortex and left temporal cortex in AD ($p<0.05$, corrected) (Fig. 1a, Supplementary Table 1). This voxel-wise analysis was confirmed by the ROI analysis showing that the quantitative value of [^{11}C](*R*)PK11195 BP was significantly higher in these regions in the AD group (Table 2). The analysis also showed that the level of [^{11}C]PIB BP was significantly higher in the medial and lateral parietal cortex, temporal cortex and frontal cortex in the AD group ($p<0.05$, corrected) (Fig. 1b, Supplementary Table 1). In addition, there were significant reductions in [^{18}F]FDG SUVR in the medial and lateral parietal cortex, temporal cortex and frontal cortex in the AD group compared to the healthy control group ($p<0.05$, corrected) (Fig. 1c, Supplementary Table 1). These findings in AD patients in comparison with healthy subjects were all consistent with the previous literature. Figure 2 shows a sample of PET parametric images of [^{11}C](*R*)PK11195 BP (Fig. 2a), [^{11}C]PIB BP (Fig. 2b) and [^{18}F]FDG SUVR (Fig. 2c) in AD patient 2.

Clinico-biotracer correlation in the AD group

Based on the present SPM results and previous literature [8–13, 27], we focused on the levels of tracer accumulation in the ACC, PCC, Prec, SFC (BA9), MFC (BA9), PHC and Hip, all of which are particularly affected in the AD brain. Pearson correlation analysis showed that there were significant negative correlations between MMSE scores and [^{11}C](*R*)PK11195 BPs in the left ACC ($r=-0.90$, $p<0.05$, corrected), left Prec ($r=-0.80$, $p<0.05$, corrected), left Hip ($r=-0.79$, $p<0.05$, corrected) and left MFC (BA9) ($r=-0.94$, $p<0.05$, corrected) in the AD group (Fig. 3, Supplementary Table 2).

Other clinical parameters failed to correlate with the levels of [^{11}C](*R*)PK11195 and [^{11}C]PIB binding in any region (data not shown). The MMSE score tended to

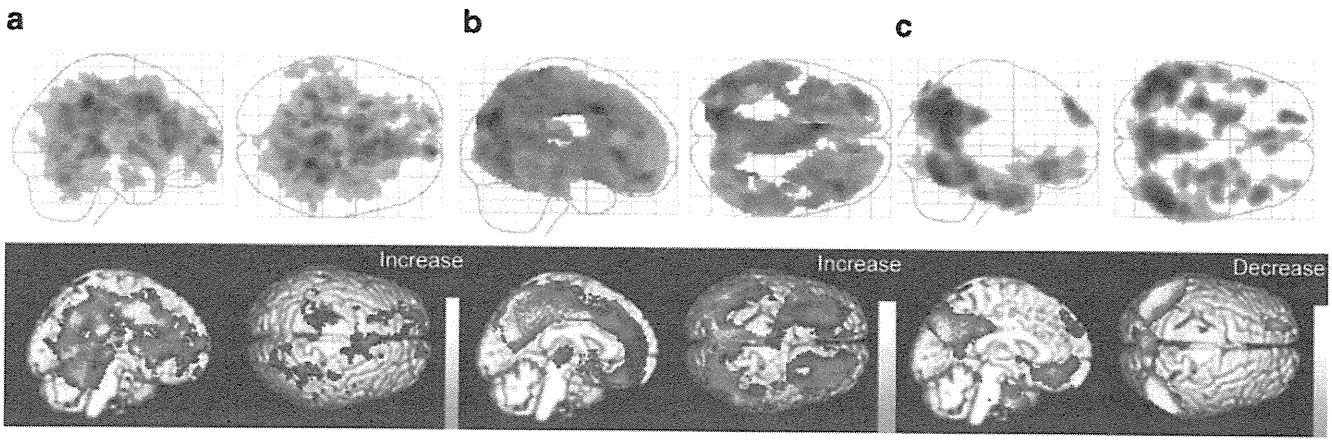

Fig. 1 Results of SPM analyses. The regions with statistically significant increases in [^{11}C](*R*)PK11195 BP (**a**) and [^{11}C]PIB BP (**b**) and decrease in [^{18}F]FDG SUVR (**c**) in AD patients compared with healthy control subjects ($p<0.05$, corrected). The *upper images* show glass brains and *lower images* denote the rendering of PET and MRI fusions. The *colour bar* denotes levels of [^{11}C](*R*)PK11195 BP, [^{11}C]PIB BP and [^{18}F]FDG SUVR

Table 2 Levels of all PET measures in the AD and control groups

Region		[^{11}C](*R*)PK11195 BP		[^{11}C]PIB BP		[^{18}F]FDG SUVR	
		AD	HC	AD	HC	AD	HC
ACC	Mean	0.39*	0.13	0.81*	0.20	1.00	1.06
	SD	0.17	0.09	0.24	0.11	0.08	0.06
		R: 0.50, L: 0.29	R: 0.14, L: 0.11	R: 0.84, L: 0.78	R: 0.20, L: 0.19	R: 0.93, L: 1.06	R: 1.05, L: 1.06
PCC	Mean	0.30*	0.04	1.04*	0.25	1.03*	1.50
	SD	0.21	0.03	0.26	0.11	0.13	0.11
		R: 0.26, L: 0.34	R: 0.01, L: 0.07	R: 1.03, L: 1.05	R: 0.27, L: 0.22	R: 1.04, L: 1.02	R: 1.51, L: 1.49
PC	Mean	0.24*	0.02	0.99*	0.18	1.17*	1.49
	SD	0.11	0.03	0.32	0.07	0.13	0.11
		R: 0.20, L: 0.28	R: 0.03, L: 0.00	R: 1.00, L: 0.98	R: 0.21, L: 0.14	R: 1.14, L: 1.19	R: 1.51, L: 1.46
Hip	Mean	0.34	0.20	0.31*	0.17	0.81*	0.99
	SD	0.11	0.13	0.16	0.13	0.16	0.06
		R: 0.33, L: 0.34	R: 0.22, L: 0.17	R: 0.33, L: 0.29	R: 0.14, L: 0.18	R: 0.81, L: 0.80	R: 0.96, L: 1.02
PHC	Mean	0.32*	0.04	0.40*	0.16	0.76*	1.06
	SD	0.12	0.06	0.16	0.08	0.11	0.07
		R: 0.32, L: 0.33	R: 0.01, L: 0.07	R: 0.37, L: 0.43	R: 0.15, L: 0.16	R: 0.76, L: 0.76	R: 1.06, L: 1.07
SFC	Mean	0.24	0.11	0.89*	0.16	1.04*	1.18
	SD	0.14	0.07	0.27	0.08	0.10	0.08
		R: 0.20, L: 0.27	R: 0.13, L: 0.09	R: 0.88, L: 0.91	R: 0.16, L: 0.17	R: 1.05, L: 1.03	R: 1.19, L: 1.17
MFC	Mean	0.28*	0.07	0.78*	0.16	1.09*	1.31
	SD	0.12	0.04	0.23	0.08	0.14	0.10
		R: 0.30, L: 0.25	R: 0.06, L: 0.07	R: 0.76, L: 0.79	R: 0.16, L: 0.17	R: 1.10, L: 1.08	R: 1.31, L: 1.31

The data on both hemispheres were averaged in each region and expressed as mean ± SD

AD Alzheimer's disease, *HC* healthy control, *ACC* anterior cingulate cortex, *PCC* posterior cingulate cortex, *Prec* precuneus, *SFC* superior frontal cortex, *MFC* middle frontal cortex, *Hip* hippocampus, *PHC* parahippocampal cortex, *R* right, *L* left

*$p<0.05$, corrected, vs healthy controls

correlate with [^{18}F]FDG SUVR in the hypometabolic regions (Supplementary Table 2)

Relationship between microglia activation and Aβ accumulation in the AD group

Direct comparisons showed a significant negative correlation between [^{11}C](*R*)PK11195 BPs and [^{11}C]PIB BPs in the PCC (left: $r=-0.84$, right: $r = -0.90$, $p<0.05$, corrected) (Fig. 4, Supplementary Table 2). There was a tendency toward negative correlation between [^{11}C](*R*)PK11195 BPs and [^{11}C]PIB BPs in the left PHC, right SFC (BA9) and right MFC (BA9). No significant correlations between [^{11}C](*R*) PK11195 BPs and FDG SUVR or between [^{11}C]PIB BPs and FDG SUVR were found in any ROIs (Supplementary Table 2).

Discussion

To our knowledge, this is the first study to examine the pathophysiological conspirators in the living AD brain using PET with three tracers ([^{11}C](*R*)PK11195, [^{11}C]PIB and [^{18}F]FDG). We showed a significant increase in [^{11}C](*R*)PK11195 BP in the ACC and PCC, where there was a more robust increase in [^{11}C]PIB accumulation and marked decrease in [^{18}F]FDG uptake. This elevation of [^{11}C](*R*) PK11195 binding was consistent with the previous reports [8, 27]. In contrast to the relatively confined region of [^{11}C](*R*)PK11195 accumulation, an elevation of [^{11}C]PIB binding was found in broader brain regions such as the parietal, temporal and frontal cortices, which was also compatible with the previous results [9–12, 23, 24, 27–29]. It is generally accepted that after the reduction in [^{18}F]FDG uptake is seen in the medial parietal cortex at a very early disease stage, it then progresses to the lateral parietal and temporal cortices, and finally to the frontal cortex [30–32]. Our patients had clinically mild-to-moderate AD (MMSE scores 21.5±3.6), and the present [^{18}F]FDG uptake pattern indicated that our patients were pathophysiologically in mid-stage disease. The findings of each tracer in the current study might be consistent with those already reported, but these pathophysiological events were measured for the first

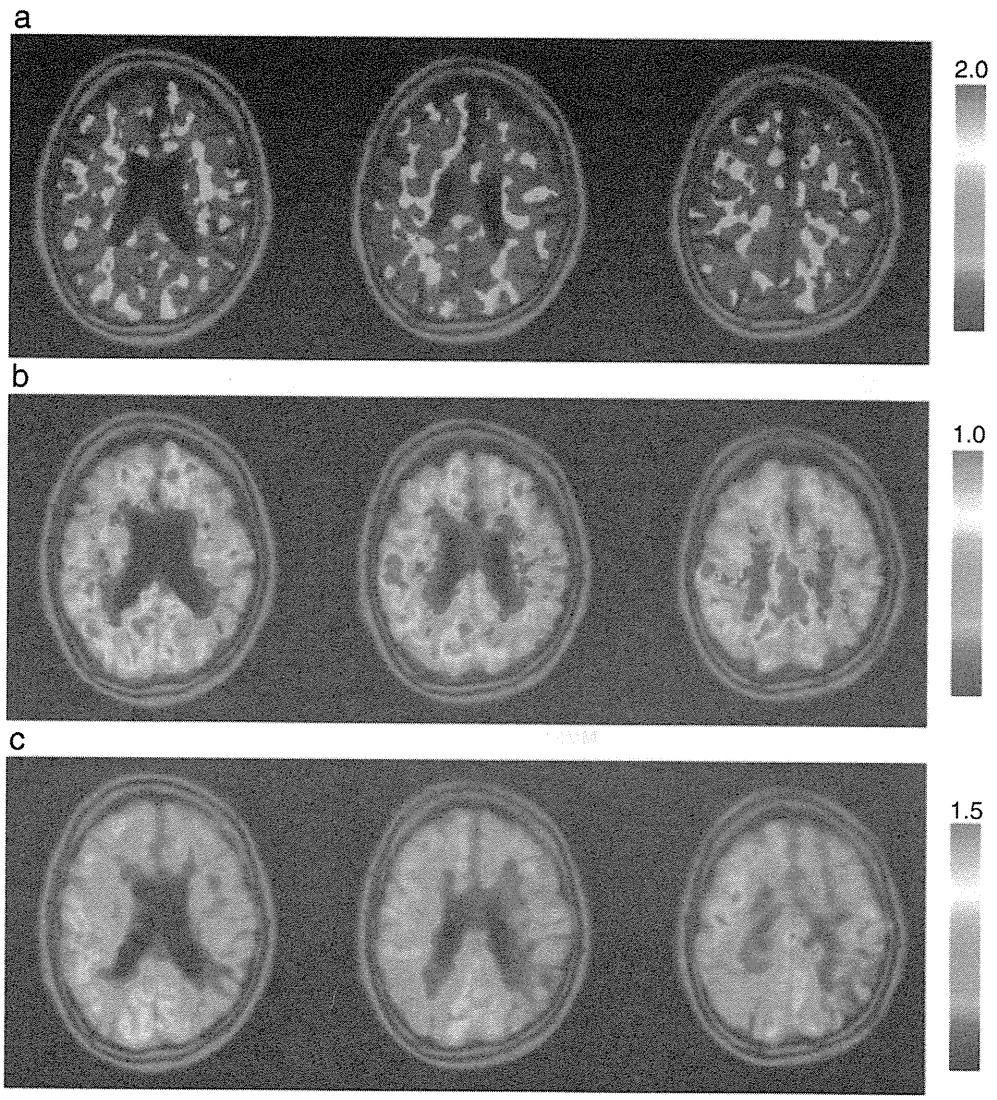

Fig. 2 Quantitative PET parametric images of an AD patient. PET parametric images of [^{11}C](*R*)PK11195 BP (**a**), [^{11}C]PIB BP (**b**) and [^{18}F]FDG SUVR (**c**) are superimposed on MRI. The *colour bars* denote levels of [^{11}C](*R*)PK11195 BP, [^{11}C]PIB BP and [^{18}F]FDG SUVR

time without any delay, i.e. we completed a whole set of neuropsychological and imaging measurements within the same day for an individual patient. Thus, the present protocol offers the great advantage of depicting pathological events occurring simultaneously in vivo in AD.

Among pathological events such as Aβ deposits, microglial activation and glucose metabolism in the AD brain, only microglial activation in the left limbic region was found to correlate with MMSE scores in the present study, which was in line with the previous report (see the supplementary data and [27]). Although glucose metabolic reduction tended to correlate with MMSE scores, no tendency of correlation was found for Aβ accumulation. This suggests that not Aβ accumulation but microglia activation is critical in the damage of neurons involved in the orchestration of cognitive function in AD. Laterality of the correlation between microglial activation and MMSE scores was observed in the present study. Lateralized [^{11}C](*R*)PK11195 binding was also reported in the previous results from Cagnin et al. [8]. In line with their report, we found a weak but significant [^{11}C](*R*)PK11195 accumulation displayed in the left temporal cortex in the SPM analysis (see Fig. 1a). The reason for this was unclear but there might have been a selection bias; all patients were right-handed. We also considered that this laterality was related to a greater vulnerability of language function in such a group, as suggested in the previous report [8]. Indeed, the present patients performed poorly on the word generation test.

There is evidence that Aβ accumulation itself is not always detrimental to the brain environment. A major component of extracellular Aβ accumulation in the AD brain is insoluble Aβ fibril and [^{11}C]PIB is reported to bind the Aβ accumulation homogeneously [11]. Because [^{11}C]PIB cannot distinguish insoluble from soluble Aβ, we do not currently know how harmful soluble Aβ can be to the brain in vivo. It has been shown that soluble and insoluble Aβ can directly or indirectly bind to receptors expressed by

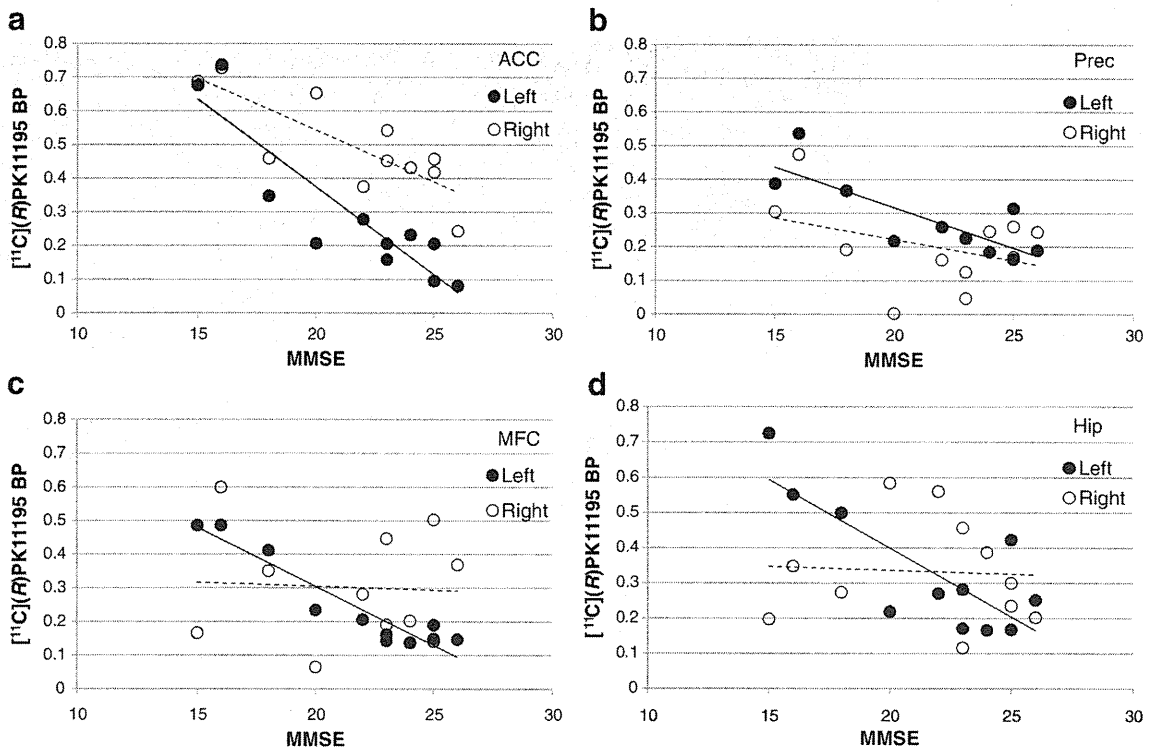

Fig. 3 Correlations between MMSE scores and regional [^{11}C](*R*)PK11195 BPs in the AD group. Scatter grams of correlations between MMSE scores and [^{11}C](*R*)PK11195 BPs in the ACC (**a**), Prec (**b**), MFC (**c**) and Hip (**d**). *Filled circles* indicate the left side of each region and *open circles* the right. *Straight lines* show significant correlations ($p<0.05$, corrected). *ACC* anterior cingulate cortex, *Prec* precuneus, *MFC* middle frontal cortex, *Hip* hippocampus

microglia through TLR, CD40 and MHC-II, which leads to activation of microglia [2–4]. Recent studies showed that soluble Aβ oligomer is involved in neurodegeneration [33, 34] and induces neuronal apoptosis mainly through activation of the sphingomyelinase-ceramide pathway [35]. Because microglial activation can be found earlier, before insoluble Aβ accumulation becomes apparent [15, 16], and soluble APP fragment activates microglia into releasing cytokines [36, 37], there is now an assumption that a change of microglial activity is related to the degree of production of soluble Aβ oligomer as a neurodegenerative trigger. In the present study, we found a significant negative correlation between microglial activation and Aβ accumulation in the PCC, which is affected early in AD [30]. Thus, it might be possible that microglial activity increases in the region at an early stage of Aβ production and subsides during the phase when neurodegeneration is predominant with large insoluble Aβ fibril deposits. Since we are currently unable to detect the amount of soluble Aβ oligomer accumulated in vivo, microglial imaging may be informative in predicting the presence of toxic substances other than Aβ fibril accumulation in AD.

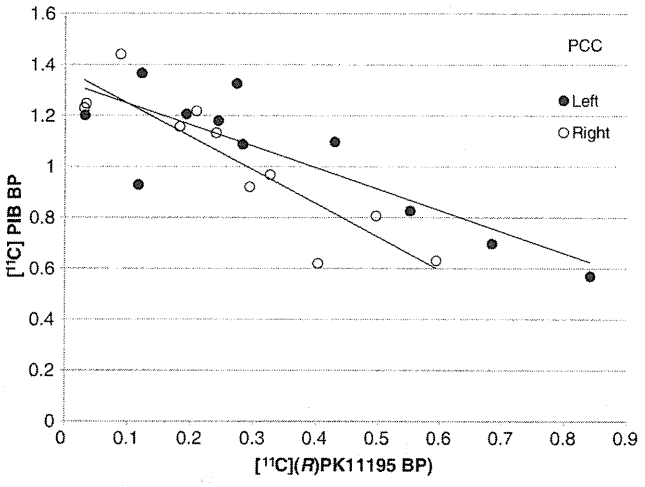

Fig. 4 Correlations between [^{11}C](*R*)PK11195 and [^{11}C]PIB BPs in the AD group. Scatter grams of correlations between [^{11}C](*R*) PK11195 BP and [^{11}C]PIB BP in the PCC. *Filled circles* indicate the left side of each region and *open circles* the right. A *straight line* denotes a significant correlation ($p<0.05$, corrected). *PCC* posterior cingulate cortex

The contention that microglial activation is important as a therapeutic target in the clinical setting may be based on the previous epidemiological observation that the incidence of AD was lower among arthritis patients with daily use of NSAIDs [38]. The efficacy of NSAIDs for AD patients is still controversial, but many reports favour their usefulness by showing that NSAID treatment delays cognitive decline

in AD patients and that the treatment suppresses activated microglia in the postmortem AD brain [39]. A series of animal experiments identified many promising drugs such as aminopyridazine which inhibits microglial activation and cytokine production from neuronal damage in rats with Aβ deposits [40] and memantine which suppresses activation of microglia by antagonizing the *N*-methyl-D-aspartate (NMDA) receptor [41]. In line with these observations, the present finding that microglial activation may play important roles in the early development of degeneration and cognitive decline would support early introduction of drugs with the capacity to suppress microglial activation in AD. With regard to detecting early events occurring in the living AD brain, our 1-day protocol PET study is useful to disclose the level of alterations and mutual relations among pathophysiological substrates in vivo. However, a larger sample size of very early AD patients or patients with mild cognitive impairment will be necessary to clarify the long-term alteration of these substrates. In addition, the relationship between early production of soluble Aβ and microglial activation needs to be determined in the living AD brain in future.

Acknowledgments We would like to thank Dr. Mitsuo Kaneko (Kaneko Clinic), Dr. Masanobu Sakamoto and Messrs. Toshihiko Kanno and Yasuo Tanizaki (Hamamatsu Medical Center), Yutaka Naito (Japan Environment Research Corporation), Masami Futatsubashi, Akihito Oda and Ms. Tomomi Shinke (Hamamatsu Photonics KK) for their support. This work was supported by Research Grants from the Japanese Ministry of Health, Labor and Welfare, and Ministry of Economy, Trade and Industry, and NEDO and the Takeda Science Foundation.

Conflicts of interest None.

References

1. Hardy J, Selkoe DJ. The amyloid hypothesis of Alzheimer's disease: progress and problems on the road to therapeutics. Science 2002;297:353–6.
2. Wyss-Coray T. Inflammation in Alzheimer disease: driving force, bystander or beneficial response? Nat Med 2006;12:1005–15.
3. Tan J, Town T, Crawford F, Mori T, DelleDonne A, Crescentini R, et al. Role of CD40 ligand in amyloidosis in transgenic Alzheimer's mice. Nat Neurosci 2002;5:1288–93.
4. Tan J, Town T, Paris D, Mori T, Suo Z, Crawford F, et al. Microglial activation resulting from CD40-CD40L interaction after beta-amyloid stimulation. Science 1999;286:2352–5.
5. Chen K, Iribarren P, Hu J, Chen J, Gong W, Cho EH, et al. Activation of Toll-like receptor 2 on microglia promotes cell uptake of Alzheimer disease-associated amyloid beta peptide. J Biol Chem 2006;281:3651–9.
6. Richard KL, Filali M, Préfontaine P, Rivest S. Toll-like receptor 2 acts as a natural innate immune receptor to clear amyloid beta 1-42 and delay the cognitive decline in a mouse model of Alzheimer's disease. J Neurosci 2008;28:5784–93.
7. Tahara K, Kim HD, Jin JJ, Maxwell JA, Li L, Fukuchi K. Role of toll-like receptor signalling in Abeta uptake and clearance. Brain 2006;129:3006–19.
8. Cagnin A, Brooks DJ, Kennedy AM, Gunn RN, Myers R, Turkheimer FE, et al. In-vivo measurement of activated microglia in dementia. Lancet 2001;358:461–7.
9. Engler H, Forsberg A, Almkvist O, Blomquist G, Larsson E, Savitcheva I, et al. Two-year follow-up of amyloid deposition in patients with Alzheimer's disease. Brain 2006;129:2856–66.
10. Scheinin NM, Aalto S, Koikkalainen J, Lötjönen J, Karrasch M, Kemppainen N, et al. Follow-up of [11C]PIB uptake and brain volume in patients with Alzheimer disease and controls. Neurology 2009;73:1186–92.
11. Klunk WE, Engler H, Nordberg A, Wang Y, Blomqvist G, Holt DP, et al. Imaging brain amyloid in Alzheimer's disease with Pittsburgh Compound-B. Ann Neurol 2004;55:306–19.
12. Edison P, Archer HA, Hinz R, Hammers A, Pavese N, Tai YF, et al. Amyloid, hypometabolism, and cognition in Alzheimer disease: an [11C]PIB and [18F]FDG PET study. Neurology 2007;68:501–8.
13. Drzezga A, Grimmer T, Henriksen G, Stangier I, Perneczky R, Diehl-Schmid J, et al. Imaging of amyloid plaques and cerebral glucose metabolism in semantic dementia and Alzheimer's disease. Neuroimage 2008;39:619–33.
14. Jack Jr CR, Lowe VJ, Weigand SD, Wiste HJ, Senjem ML, Knopman DS, et al. Serial PIB and MRI in normal, mild cognitive impairment and Alzheimer's disease: implications for sequence of pathological events in Alzheimer's disease. Brain 2009;132:1355–65.
15. Heneka MT, Sastre M, Dumitrescu-Ozimek L, Dewachter I, Walter J, Klockgether T, et al. Focal glial activation coincides with increased BACE1 activation and precedes amyloid plaque deposition in APP[V717I] transgenic mice. J Neuroinflammation 2005;2:22.
16. Jacobsen JS, Wu CC, Redwine JM, Comery TA, Arias R, Bowlby M, et al. Early-onset behavioral and synaptic deficits in a mouse model of Alzheimer's disease. Proc Natl Acad Sci U S A 2006;103:5161–6.
17. McKhann G, Drachman D, Folstein M, Katzman R, Price D, Stadlan EM. Clinical diagnosis of Alzheimer's disease: report of the NINCDS-ADRDA Work Group under the auspices of Department of Health and Human Services Task Force on Alzheimer's Disease. Neurology 1984;34:939–44.
18. Ouchi Y, Nobezawa S, Okada H, Yoshikawa E, Futatsubashi M, Kaneko M. Altered glucose metabolism in the hippocampal head in memory impairment. Neurology 1998;51:136–42.
19. Watanabe M, Shimizu K, Omura T, Takahashi M, Kosugi T, Yoshikawa E, et al. A new high-resolution PET scanner dedicated to brain research. IEEE Trans Nucl Sci 2002;49:634–9.
20. Lammertsma AA, Hume SP. Simplified reference tissue model for PET receptor studies. Neuroimage 1996;4:153–8.
21. Banati RB, Newcombe J, Gunn RN, Cagnin A, Turkheimer F, Heppner F, et al. The peripheral benzodiazepine binding site in the brain in multiple sclerosis: quantitative in vivo imaging of microglia as a measure of disease activity. Brain 2000;123:2321–37.
22. Ouchi Y, Yoshikawa E, Sekine Y, Futatsubashi M, Kanno T, Ogusu T, et al. Microglial activation and dopamine terminal loss in early Parkinson's disease. Ann Neurol 2005;57:168–75.
23. Price JC, Klunk WE, Lopresti BJ, Lu X, Hoge JA, Ziolko SK, et al. Kinetic modeling of amyloid binding in humans using PET imaging and Pittsburgh Compound-B. J Cereb Blood Flow Metab 2005;25:1528–47.

24. Lopresti BJ, Klunk WE, Mathis CA, Hoge JA, Ziolko SK, Lu X, et al. Simplified quantification of Pittsburgh Compound B amyloid imaging PET studies: a comparative analysis. J Nucl Med 2005;46:1959–72.
25. Talairach J, Tournoux P. Co-planer stereotaxic atlas of the human brain: 3-dimensional proportional system: an approach to cerebral imaging. Stuttgart: Thieme; 1988.
26. Ouchi Y, Yoshikawa E, Okada H, Futatsubashi M, Sekine Y, Iyo M, et al. Alterations in binding site density of dopamine transporter in the striatum, orbitofrontal cortex, and amygdala in early Parkinson's disease: compartment analysis for beta-CFT binding with positron emission tomography. Ann Neurol 1999;45:601–10.
27. Edison P, Archer HA, Gerhard A, Hinz R, Pavese N, Turkheimer FE, et al. Microglia, amyloid, and cognition in Alzheimer's disease: an [11C](R)PK11195-PET and [11C]PIB-PET study. Neurobiol Dis 2008;32:412–9.
28. Wiley CA, Lopresti BJ, Venneti S, Price J, Klunk WE, DeKosky ST, et al. Carbon 11-labeled Pittsburgh Compound B and carbon 11-labeled (R)-PK11195 positron emission tomographic imaging in Alzheimer disease. Arch Neurol 2009;66:60–7.
29. Leinonen V, Alafuzoff I, Aalto S, Suotunen T, Savolainen S, Någren K, et al. Assessment of beta-amyloid in a frontal cortical brain biopsy specimen and by positron emission tomography with carbon 11-labeled Pittsburgh Compound B. Arch Neurol 2008;65:1304–9.
30. Minoshima S, Giordani B, Berent S, Frey KA, Foster NL, Kuhl DE. Metabolic reduction in the posterior cingulate cortex in very early Alzheimer's disease. Ann Neurol 1997;42:85–94.
31. Foster NL, Wang AY, Tasdizen T, Fletcher PT, Hoffman JM, Koeppe RA. Realizing the potential of positron emission tomography with 18F-fluorodeoxyglucose to improve the treatment of Alzheimer's disease. Alzheimers Dement 2008;4:S29–36.
32. Alexander GE, Chen K, Pietrini P, Rapoport SI, Reiman EM. Longitudinal PET evaluation of cerebral metabolic decline in dementia: a potential outcome measure in Alzheimer's disease treatment studies. Am J Psychiatry 2002;159:738–45.
33. Lacor PN, Buniel MC, Furlow PW, Clemente AS, Velasco PT, Wood M, et al. Abeta oligomer-induced aberrations in synapse composition, shape, and density provide a molecular basis for loss of connectivity in Alzheimer's disease. J Neurosci 2007;27:796–807.
34. Shankar GM, Li S, Mehta TH, Garcia-Munoz A, Shepardson NE, Smith I, et al. Amyloid-beta protein dimers isolated directly from Alzheimer's brains impair synaptic plasticity and memory. Nat Med 2008;14:837–42.
35. Malaplate-Armand C, Florent-Béchard S, Youssef I, Koziel V, Sponne I, Kriem B, et al. Soluble oligomers of amyloid-beta peptide induce neuronal apoptosis by activating a cPLA2-dependent sphingomyelinase-ceramide pathway. Neurobiol Dis 2006;23:178–89.
36. Szczepanik AM, Rampe D, Ringheim GE. Amyloid-beta peptide fragments p3 and p4 induce pro-inflammatory cytokine and chemokine production in vitro and in vivo. J Neurochem 2001;77:304–17.
37. Barger SW, Harmon AD. Microglial activation by Alzheimer amyloid precursor protein and modulation by apolipoprotein E. Nature 1997;388:878–81.
38. McGeer PL, McGeer E, Rogers J, Sibley J. Anti-inflammatory drugs and Alzheimer disease. Lancet 1990;335:1037.
39. Mackenzie IR. Postmortem studies of the effect of anti-inflammatory drugs on Alzheimer-type pathology and associated inflammation. Neurobiol Aging 2001;22:819–22.
40. Craft JM, Watterson DM, Frautschy SA, Van Eldik LJ. Aminopyridazines inhibit beta-amyloid-induced glial activation and neuronal damage in vivo. Neurobiol Aging 2004;25:1283–92.
41. Rosi S, Ramirez-Amaya V, Vazdarjanova A, Esparza EE, Larkin PB, Fike JR, et al. Accuracy of hippocampal network activity is disrupted by neuroinflammation: rescue by memantine. Brain 2009;132:2464–77.

Behavioral/Systems/Cognitive

Effects of Brain Amyloid Deposition and Reduced Glucose Metabolism on the Default Mode of Brain Function in Normal Aging

Mitsuru Kikuchi,[1] Tetsu Hirosawa,[2] Masamichi Yokokura,[3] Shunsuke Yagi,[3] Norio Mori,[3] Etsuji Yoshikawa,[6] Yujiro Yoshihara,[3] Genichi Sugihara,[3] Kiyokazu Takebayashi,[3] Yasuhide Iwata,[3] Katsuaki Suzuki,[3] Kazuhiko Nakamura,[3] Takatoshi Ueki,[5] Yoshio Minabe,[2] and Yasuomi Ouchi[4]

[1]Research Center for Child Mental Development and [2]Department of Psychiatry and Neurobiology, Graduate School of Medical Science, Kanazawa University, Kanazawa 920-8641, Japan, [3]Department of Psychiatry and Neurology, [4]Medical Photonics Research Center, and [5]Department of Neuroanatomy, Hamamatsu University School of Medicine, Hamamatsu 431-3192, Japan, and [6]Central Research Laboratory, Hamamatsu Photonics K.K., Hamamatsu 434-8601, Japan

Brain β-amyloid (Aβ) deposition during normal aging is highlighted as an initial pathogenetic event in the development of Alzheimer's disease. Many recent brain imaging studies have focused on areas deactivated during cognitive tasks [the default mode network (DMN), i.e., medial frontal gyrus/anterior cingulate cortex and precuneus/posterior cingulate cortex], where the strength of functional coordination was more or less affected by cerebral Aβ deposits. In the present positron emission tomography study, to investigate whether regional glucose metabolic alterations and Aβ deposits seen in nondemented elderly human subjects ($n = 22$) are of pathophysiological importance in changes of brain hemodynamic coordination in DMN during normal aging, we measured cerebral glucose metabolism with [^{18}F]FDG, Aβ deposits with [^{11}C]PIB, and regional cerebral blood flow during control and working memory tasks by $H_2{}^{15}O$ on the same day. Data were analyzed using both region of interest and statistical parametric mapping. Our results indicated that the amount of Aβ deposits was negatively correlated with hemodynamic similarity between medial frontal and medial posterior regions, and the lower similarity was associated with poorer working memory performance. In contrast, brain glucose metabolism was not related to this medial hemodynamic similarity. These findings suggest that traceable Aβ deposition, but not glucose hypometabolism, in the brain plays an important role in occurrence of neuronal discoordination in DMN along with poor working memory in healthy elderly people.

Introduction

Accumulated evidence obtained by functional brain imaging has revealed two dominant domains that act in opposite ways to each other. One set of brain areas shows increases in activity, while the other set of areas shows decreases in activity during performance of a wide range of different types of cognitive task (Fox et al., 2005). The former set of brain areas includes the dorsolateral prefrontal cortex (DLPFC) and the precentral and inferior parietal cortices (Cabeza and Nyberg, 2000; Owen et al., 2005). The latter set of brain areas includes the precuneus and posterior cingulate cortex (preC/PCC), and a medial frontal region including parts of medial frontal gyrus and ventral anterior cingulate cortex (MFG/vACC) (Raichle, 1998; Gusnard and Raichle, 2001; Mazoyer et al., 2001; Simpson et al., 2001a; Fox et al., 2005). These latter task-negative responses have been proposed as the default mode of brain function (Simpson et al., 2001a), and coactivation in a distributed network [i.e., the default mode network (DMN)] in these cortical regions has been revealed (Greicius et al., 2003). Specifically, the posterior part of the DMN (i.e., precuneus) has been recognized as the region with early changes in glucose metabolism (Silverman et al., 2001; Drzezga et al., 2003) as well as Aβ deposition (Mintun et al., 2006) in Alzheimer's disease (AD). Recent imaging studies also showed that the DMN function was impaired in AD patients and altered in healthy elderly people by some degree of Aβ deposition (Greicius et al., 2004; Supekar et al., 2008; Hedden et al., 2009; Sperling et al., 2009; Zhang et al., 2009; Sheline et al., 2010). Therefore we hypothesized that, even in the healthy older individuals, altered default mode of brain function is associated with some degree of amyloid pathology, of reduction in glucose metabolism, and of deterioration of cognitive performance, which may be central to aging effect on slowness of thoughts in the elderly. However, no previous study has demonstrated them all in the same subjects. The main purpose of the present study was to examine whether the DMN measured by the steady-state brain hemodynamic configuration is relevant to the cognitive decline,

Received May 20, 2011; accepted June 14, 2011.

Author contributions: M.K., N.M., and Y.O. designed research; M.K., T.H., M.Y., S.Y., E.Y., Y.Y., G.S., K.T., Y.I., K.S., K.N., T.U., Y.M., and Y.O. performed research; M.K. contributed unpublished reagents/analytic tools; M.K., T.H., E.Y., T.U., and Y.O. analyzed data; M.K. and Y.O. wrote the paper.

This work was supported by the Ishikawa High-Tech Sensing Cluster Grant (Knowledge Cluster Initiative from the Japanese Ministry of Education, Culture, Sports, Science, and Technology), New Energy and Industrial Technology Development Organization, and the Takeda Science Foundation. We thank Toshihiko Kanno, Yasuo Tanizaki (Hamamatsu Medical Center), Masami Futatsubashi (Hamamatsu Photonics KK), and Yutaka Naito (Japan Environment Research Corporation) for their support.

The authors declare no competing financial interests.

Correspondence should be addressed to Dr. Yasuomi Ouchi, Department of Biofunctional Imaging, Medical Photonics Research Center, Hamamatsu University School of Medicine, 1-20-1 Handayama, Higashi-ku, Hamamatsu 431-3192, Japan. E-mail: ouchi@hama-med.ac.jp.

DOI:10.1523/JNEUROSCI.2535-11.2011

 0270-6474/11/3111193-07$15.00/0

glucose hypometabolism, and amyloid burden under normal aging. The advantage of the present study was that measurement of these biological parameters in the same subjects on the same day allowed us to compare the default mode of brain function with amount of Aβ deposit by [^{11}C] Pittsburgh compound B (PIB)-positron emission tomography (PET) and with glucose metabolism by [^{18}F] fluorodeoxyglucose (FDG)-PET directly. To evaluate the DMN under steady-state hemodynamic configurations during various cognitive conditions (the mean of phasic variations), $H_2{}^{15}O$-PET was used for assessment of steady-state cerebral blood flow.

Materials and Methods

Participants. We examined 22 healthy elderly subjects (9 men and 13 women; mean age 68.0 ± 7.28 years) (Table 1). None of the subjects had any personal or family history of psychiatric or neurological diseases. The exclusion criteria were (1) dysfunction or difficulty in independence in their daily lives, or loss of social interaction in their community, as assessed by Clinical Dementia Rating (CDR) (Morris, 1993) ≥0.5 or Functional Assessment Staging of Alzheimer's Disease (FAST) (Reisberg, 1986) ≥2; (2) presence of significant white matter microvascular changes on magnetic resonance imaging (MRI) over and above a few scattered lacunas compatible with normal aging; (3) drinking large amounts of alcohol regularly or smoking; (4) taking any medication for at least 8 weeks before the examination; and (5) untreated hypertension or diabetes. The present study was approved by the Ethics Committee of Hamamatsu Medical Center, and written informed consent was obtained from all participants before enrollment.

MRI scanning. All participants underwent three-dimensional MRI just before PET measurement. Here, a static magnet (0.3 T MRP7000AD; Hitachi) was used in three-dimensional mode (Ouchi et al., 2001).

Working memory task. Visual tasks were presented on a liquid crystal screen in front of subjects during PET scanning. One type of resting control condition and two types of working memory task were used; as shown in Figure 1, one was the simple visual working memory task (WM task) and the other was the visual working memory with mental rotation (RWM task).

Regional cerebral blood flow measurement using PET scan during working memory task. We used a high-resolution brain PET scanner (SHR12000; Hamamatsu Photonics K.K.) (Ouchi et al., 1999). After head fixation using a thermoplastic face mask and a 10 min transmission scan, we performed quantitative measurement of regional cerebral blood flow (rCBF) in the conventional manner (Herscovitch et al., 1983; Ouchi et al., 2001). Nine 1 min PET scans for rCBF were performed under various conditions, as shown in Figure 1*B*. The dose of $H_2{}^{15}O$ injected was 4 MBq/kg per scan.

Image data acquisition. After measurement of rCBF during working memory, with a rest period of 1 h, 40 serial PET scans (time frames: 12 × 10, 18 × 60, and 10 × 300 s) were performed for 70 min after injection of 5 MBq [^{11}C]PIB/kg. Later, a static 15 min PET scan was performed 45 min after injection of 1.2 MBq/kg dose of [^{18}F]FDG.

Image data processing. To evaluate rCBF, $H_2{}^{15}O$-PET images from each participant were individually adjusted for mean image (normalized rCBF) (Ouchi et al., 2001). To evaluate glucose metabolism, a semiquantitative ratio index of [^{18}F]FDG was calculated as standardized uptake value ratio (SUVR) (Ouchi et al., 2009). To evaluate Aβ accumulation, a semiquantitative ratio index of [^{11}C] PIB binding potentials was estimated as SUVR (Yokokura et al., 2011).

ROI analysis. PET images using $H_2{}^{15}O$ were realigned, and all PET images, including [^{18}F]FDG-SUVR and [^{11}C]PIB-SUVR images, were spatially normalized into the Montreal Neurological Institute (MNI) coordinate system using [^{18}F]FDG-PET template for $H_2{}^{15}O$ and [^{18}F]FDG images and early summation [^{11}C]PIB PET template for [^{11}C]PIB images to calculate the warping parameters (Nelissen et al., 2007), and smoothed with a 8 × 8 × 8 mm Gaussian kernel using SPM8 (Wellcome Department of Cognitive Neurology, http://www.fil.ion.ucl.ac.uk/spm/software/spm8/). The use of a thermoplastic face mask and three-dimensional laser markers enabled us to keep the subjects' heads fixed in the same position during a series of all PET measurements (Ouchi et al., 2006). For $H_2{}^{15}O$ and [^{18}F] FDG images, proportional scaling was used to correct for within-session variations in global signals for each adjusted mean image. Regional data for CBF, [^{11}C]PIB index, and [^{18}F]FDG index were determined automatically for each participant using MarsBaR, which provided us with a sophisticated template for regions of interest (ROIs) on statistical parametric mapping (SPM) normalized images [MARSeille Boîte À Région d'Intérêt (Brett et al., 2002)]. The details of this ROI procedure have been reported previously (Tzourio-Mazoyer et al., 2002).

Similarity index in the default mode network. To evaluate functional coupling between MFG/vACC and preC/PCC (or level of frontoposterior disengagement in DMN), we used Spearman's rank correlation coefficient as a similarity index, in which a higher value of this index denoted a higher functional engagement in DMN. We used this coeffi-

Table 1. Demographic characteristics of all subjects

Group	Healthy subjects
Total number	22
Male/female	9/13
Age (years)	68.0 (57–81)
Education (years)	10.7 (8–16)
CDR	0 (0)
FAST	1 (1)
MMSE score	28.8 (26–30)
Cubic copying test	
Point of connection	8 (8)[a]
Plane-drawing errors	0 (0)[b]
Lexical fluency	3 (3)[c]
Correct answer for WM and RWM test (%)	94.4 (86.7–100.0)[d]

MMSE, Mini-Mental State Examination. [a]Eight points represents a perfect score (Maeshima et al., 1997). [b]Zero points represents a perfect score (Maeshima et al., 1997). [c]Three points represents a perfect score (Frontal Assessment Battery subtest) (Dubois et al., 2000). [d]One hundred percent represents a perfect score. Except for the first two rows, values are given as mean (range).

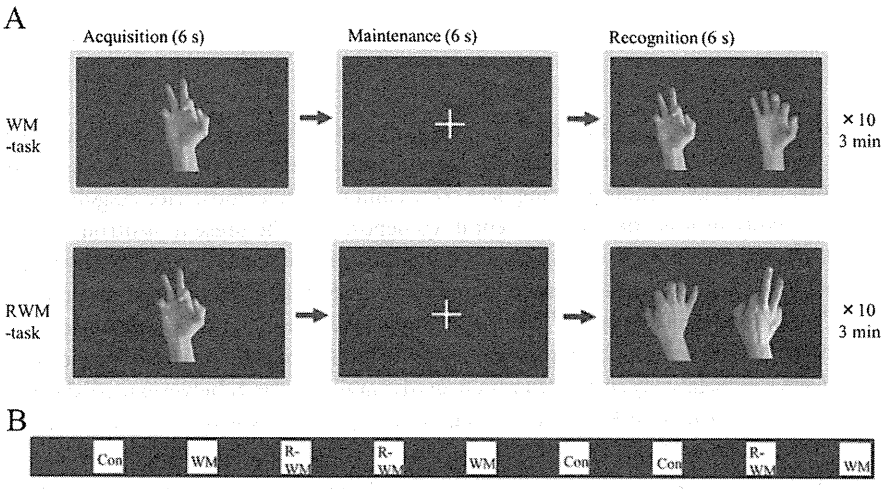

Figure 1. Task paradigm. ***A***, Subjects performed two types of working memory task; one was a simple visual WM task and the other was a visual RWM task in which subjects were asked to select the correct picture with the same hand flipped over from the palm side (acquisition) to the rear (recognition). For the resting control condition (Con), subjects were asked to look at a cross mark centered in the screen. To avoid drowsiness under control conditions, subjects were instructed to press a button in the right or left hand every 18 s. ***B***, Each condition continued for 3 min and each interval lasted for 7 min with the eyes closed (black square).

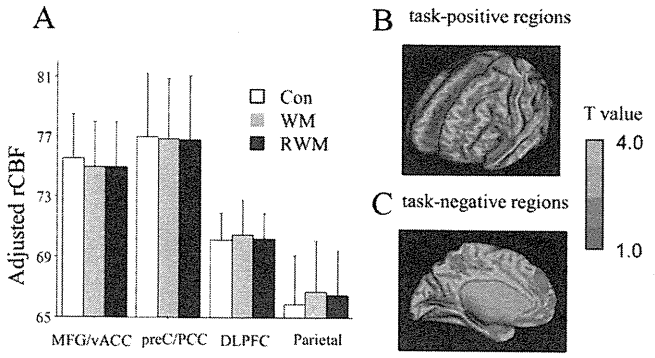

Figure 2. *A*, Results of ROI analyses. Three-way ANCOVA showed a significant interaction between region and condition effects (Table 2). This interaction was due to the inverse hemodynamic responses to memory task between ROIs (i.e., medial vs lateral ROIs). Error bars indicate 1 SD. *B*, Exploratory SPM analyses ($p < 0.001$, uncorrected). Significant elevation of rCBF in DLPFC and parietal and occipital cortices during memory conditions (WM and RWM tasks) as compared with control conditions. *C*, Significant reduction of rCBF in MFG, preC, and occipital cortex during memory conditions (WM and RWM tasks) as compared with control conditions. Con, Control condition.

cient because it is available without knowledge of the joint probability distribution of these two regions.

Statistics for ROI analysis. For the rCBF variable, three-way analysis of covariance (ANCOVA) was performed (ROI × condition × gender). Two factors were within subjects for region effect (MFG/vACC vs preC/PCC vs DLPFC vs parietal cortex) and condition effect (control vs WM task vs RWM task). One factor was between subjects for gender effect (male vs female). To remove the effect of age, we defined age as a covariate. Statistical significance was defined as $p < 0.05$. Relationships between dependent variables (i.e., [^{11}C]PIB or [^{18}F]FDG index from 11 ROI) and independent variables (hemodynamic similarity index, working memory performance, or age) were assessed using Spearman's rank correlation coefficient. Statistical significance was defined as $p < 0.0045$ because of multiple comparisons (11 ROIs). In addition, the effects of age on these independent variables were assessed using Spearman's rank correlation coefficient, and gender differences in these independent variables were assessed using Mann–Whitney *U* test. Statistical significance was defined as $p < 0.05$.

Statistics for voxelwise analysis. SPM8 was used for voxelwise analysis. All [^{15}O]rCBF, [^{11}C]PIB-SUVR, and [^{18}F]FDG-SUVR parametric images were first normalized to the MNI space and smoothed with an isotropic Gaussian kernel of 8 mm (same method with ROI analysis). The between-condition comparisons for rCBF were performed using the flexible factorial model with a statistical threshold set at $p = 0.001$ uncorrected for peak height. Confounding factors of age and gender were included in the model. Voxel-based correlations were computed between rCBF similarity index and [^{11}C]PIB-SUVR and [^{18}F]FDG-SUVR parametric images using the multiple regression model with the statistical threshold set at $p = 0.001$ uncorrected for peak height. Confounding factors of age and gender were also included in the model.

Results

Changes in regional cerebral blood flow

rCBF was estimated in the brain regions that were a priori considered important in DMN (MFG/vACC and preC/PCC as task-negative regions, DLPFC and parietal lobes as task-positive regions) for each participant. Three-way ANCOVA showed a significant interaction effect between ROI and condition ($F = 2.28$; $p = 0.041$) (Fig. 2*A*, Table 2). As shown in Figure 2*A*, this interaction was due to the inverse hemodynamic responses to memory task between ROIs (especially medial vs lateral ROIs). Whole-brain SPM analysis revealed significant elevation of rCBF in superior, middle, and inferior frontal gyri, superior parietal lobules, middle and inferior occipital gyri, and fusiform gyrus (Fig. 2*B*), and significant

Table 2. Three-way ANCOVA for rCBF hemodynamics

	Region effect		Condition effect		Gender effect		Interaction: region × condition	
	F value	*p* value	*F* value	*p* value	*F* value	*p* value	*F* value	*p* value
rCBF	5.17	0.003	3.31	0.047	0.51	n.s.	2.28	0.041

We used the ANCOVA in order to remove the effect of a covariate (age). Two factors for within subject: region effect, MFG/vACC versus preC/PCC versus DLPFC versus parietal cortex; condition effect, control versus WM-task versus RWM-task. One factor for between subjects: gender effect, male versus female. Covariance: age. n.s., No significance.

reduction in superior, medial, and inferior frontal gyri, uncus, precentral gyrus, superior and middle temporal gyri, angular gyrus, and precuneus (Fig. 2*C*) during working memory as compared with control conditions.

Correlations between regional [^{11}C]PIB-SUVR and hemodynamic similarity index

Figure 4*A* denotes Spearman's rank correlation between regional [^{11}C]PIB-SUVR (separating the whole brain into 11 regions) and hemodynamic similarity index. PIB-SUVR in the whole cerebral cortex, MFG/vACC, and middle temporal and inferior temporal cortices showed a negative correlation with the hemodynamic similarity in DMN ($\rho = -0.640$, $p = 0.0034$ for the whole brain as shown in Fig. 3*A*). Whole-brain SPM correlation analysis showed that PIB uptake in the cingulate gyrus, parahippocampal gyrus, fusiform gyrus, cuneus, insula, and lentiform nucleus were correlated negatively with the similarity index (Table 3, Fig. 4*B*).

Correlations between regional [^{18}F]FDG-SUVR and hemodynamic similarity index

Although ROI analysis failed to demonstrate any correlation between adjusted regional FDG-SUVR and hemodynamic similarity index (Fig. 5*A*), we continued to perform voxel-based analysis. As shown in Table 3 and Figure 5*B*, relatively higher FDG-SUVR in the temporooccipital region (outside the medial DMN region) was associated with higher similarity index.

Correlations between working memory performance and hemodynamic similarity index, regional [^{11}C]PIB-SUVR, or regional [^{18}F]FDG-SUVR

Spearman's rank correlation coefficient showed the number of correct answers correlated positively with the similarity index in DMN ($\rho = 0.646$, $p = 0.0031$) (Fig. 3*B*), and negatively with the PIB-SUVR in middle temporal cortices (Fig. 4*A*). There was no significant correlation between cognitive performance and regional FDG-SUVR (Fig. 5*A*).

Effect of age on hemodynamic similarity index, working memory performance, regional [^{11}C]PIB-SUVR, or regional [^{18}F]FDG-SUVR

Spearman's rank correlation coefficient showed no significant correlation between age and similarity index ($\rho = 0.274$, $p > 0.05$), working memory performance ($\rho = 0.002$, $p > 0.05$), or regional [11C]PIB-SUVR in all 11 ROIs ($p > 0.0045$) (Fig. 4*A*). There was no brain region but superior temporal cortex, in which [18F]FDG-SUVR was significantly correlated with age ($\rho = -0.627$, $p = 0.0040$).

Effect of gender difference on age, hemodynamic similarity index, and working memory performance

Mann–Whitney *U* test failed to demonstrate any significant gender differences for age ($U = 52.5$, $p > 0.05$), similarity

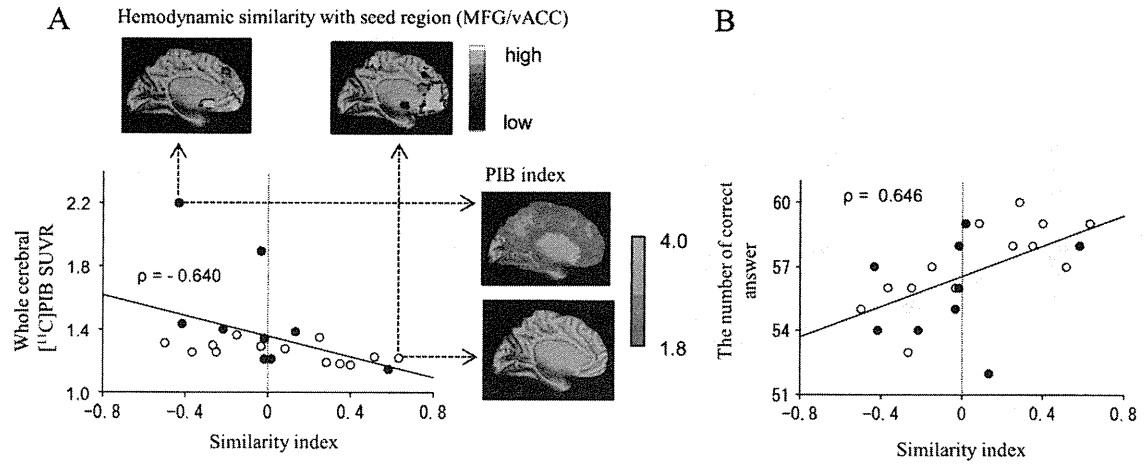

Figure 3. *A*, [^{11}C]PIB-SUVR in the whole cerebral cortex was correlated negatively with the similarity index ($\rho = -0.640, p = 0.0034$). Representative images for opposite changes between [^{11}C]PIB index and hemodynamic similarity were shown in two subjects. A subject (top left) with the higher PIB index shows the lower hemodynamic similarity in preC/PCC with seed region (MFG/vACC), whereas the other subject (bottom right) with the lower PIB shows the higher similarity in preC/PCC. ***B***, The number of correct answers to working memory task was correlated positively with the similarity index between MFG/vACC and preC/PCC ($\rho = 0.646, p = 0.0031$).

Table 3. Brain regions with significant[a] relationships between [^{11}C]PIB-SUVR or [^{18}F]FDG-SUVR and hemodynamic similarity index

Brain area	BA	Hemisphere	Coordinate[b]			z score	Cluster size
			x	y	z		
Negative correlation between [^{11}C]PIB-SUVR and similarity index							
Temporal Lobe							
Fusiform Gyr.	37	R	38	−52	−8	3.64	161
Limbic Lobe							
Cingulate Gyr.	24	R	15	−7	33	5.65	2982
Cingulate Gyr.	31	L	−20	−36	33	5.07	3265
Parahippocampal Gyr.	28	L	−22	−13	−17	4.63	297
Parahippocampal Gyr.	28	R	13	−21	−19	4.29	1220
Cingulate Gyr.	30	L	−27	−65	12	3.72	91
Cingulate Gyr.	29	R	3	−48	8	3.57	62
Occipital Lobe							
Cuneus	17	R	24	−79	6	3.54	118
Sublobar							
Lentiform nucleus	—	L	−8	1	0	3.68	51
Insula	13	L	−43	−7	15	3.49	52
Positive correlation between [^{18}F]FDG-SUVR and dissimilarity index							
Temporal Lobe							
Middle temporal Gyr.	19	L	−40	−79	20	3.54	33
Occipital Lobe							
Middle temporal Gyr.	19	R	40	−60	14	3.60	65
Middle temporal Gyr.	19	L	−41	−60	16	3.39	39

[a]Statistical significance was assumed at an individual voxel level of $p < 0.001$, uncorrected. [b]Talairach and Tournoux brain atlas coordinates: x = distance in millimeters to the right (+) or left (−) side of the midline; y = distance anterior (+) or posterior (−) to the anterior commissure; z = distance superior (+) or inferior (−) to a horizontal plane through the anterior and posterior commissures. BA, Brodmann's area; Gyr., gyrus.

index ($U = 48.5$, $p > 0.05$), and working memory performance ($U = 39.5$, $p > 0.05$).

Discussion

Hemodynamic response, similarity index, and [^{11}C]PIB uptake

Our hemodynamic study focusing on the four loci showed two opposing hemodynamic responses; i.e., DLPFC and parietal cortex were activated during cognitive tasks, while MFG/vACC and preC/PCC were deactivated (Fig. 2). This disparity was replicated by other tasks in previous studies (Raichle, 1998; Mazoyer et al., 2001; Simpson et al., 2001a; Buckner et al., 2005; Fox et al., 2005). These hemodynamic responses were shown to disappear under pathological conditions, such as mild cognitive impairment (MCI) and AD (Lustig et al., 2003; Petrella et al., 2007), suggesting disruption of brain default mode. Indeed, it was of particular interest that the anatomical pattern of high Aβ deposits in the AD brain was very similar to the anatomical pattern of the default mode activity, especially in the medial posterior part of the brain preC/PCC (Buckner et al., 2005). Even in nondemented elderly individuals, high levels of Aβ deposits were shown to be related to altered DMN activity on functional magnetic resonance imaging (fMRI) (Sperling et al., 2009). In addition, we found that the similarity index between MFG/vACC and preC/PCC across the rest and task conditions was negatively correlated with PIB-SUVR (Fig. 4*A*,*B*) and positively correlated with the working memory performance (Fig. 3*B*). These results suggest that Aβ deposition, if any, during normal aging could affect DMN activity and deteriorate cognitive performance. As shown in Table 2

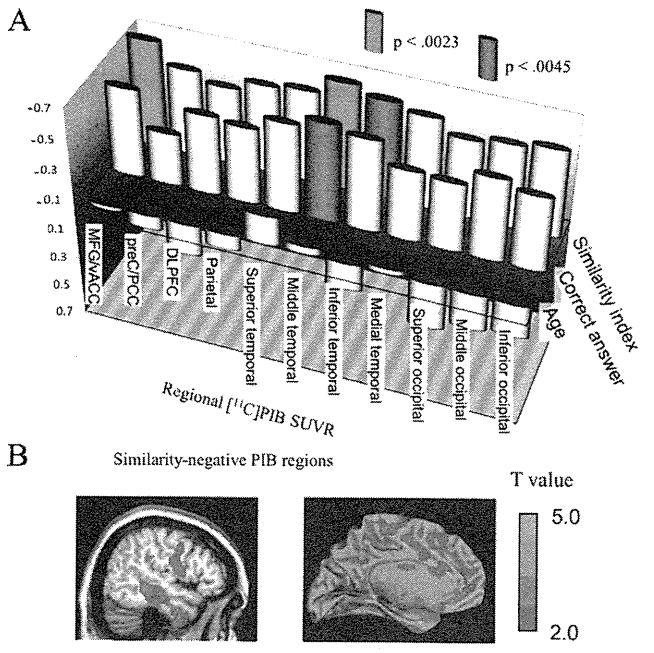

Figure 4. *A*, Spearman's rank correlation coefficient between adjusted regional [^{11}C]PIB-SUVR and hemodynamic similarity index, cognitive performance (the number of correct answers), or age. *B*, Exploratory SPM analyses. [^{11}C]PIB-SUVR in the MFG, cingulate gyrus, and temporal lobes showed negatively correlations with the similarity index.

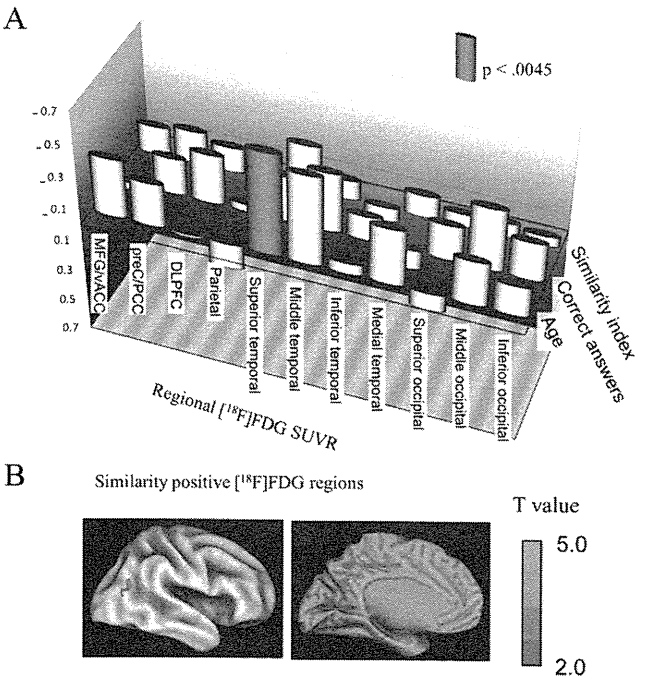

Figure 5. *A*, Spearman's rank correlation coefficient between adjusted regional [^{18}F]FDG-SUVR and hemodynamic similarity index, cognitive performance (the number of correct answers), or age. *B*, Exploratory SPM analyses. [^{18}F]FDG-SUVR in the temporooccipital regions was positively correlated with the similarity index.

and Figures 4 and 5, effects of age and gender were negligible in this study, suggesting again that Aβ deposition is of a pathophysiological value for the DMN malfunction. However, to answer why women suffer more from AD than men (Jorm and Jolley, 1998; Fratiglioni et al., 2000), a larger number of participants with a broader age range would be necessary for clarification of gender effect.

The steady state of the brain

Imaging of a physiological baseline state of the brain depends on the imaging modality used, such as PET or MRI. PET is insensitive to second time scale fluctuations in brain physiology, but it can capture the steady state of the brain perfusion and metabolism as a stable unit parameter (Raichle et al., 1983; Ouchi et al., 2001). Considering the role of regional engagement of the basal brain function, depiction of the steady state in the target brain region may sometimes be preferable. In particular, physiological noise, such as respiratory or cardiac noise, can reduce power or yield artifactual correlations in functional connectivity studies (Lowe et al., 1998; Raj et al., 2001; Birn et al., 2006; Lund et al., 2006), and these noise sources would become artifacts that affect DMN (Birn et al., 2006). The 1 min scan of the steady state used in the present study minimized the chances of physiological artificial noise or mental unsteadiness noise. The similarity index, therefore, reflects the steady-state conditions of the brain activity (i.e., resting and working memory conditions). Although the physiological significance may be different from the fMRI methods that have been reported in previous studies (Hampson et al., 2006; Sheline et al., 2010), our results using a similarity index were consistent with those of recent fMRI studies as follows. Performance on the working memory task was positively correlated with the strength of the functional connectivity between the PCC and MFG/vACC in nine healthy subjects (Hampson et al., 2006), and higher functional connectivity between preC and anterior cingulate was observed in nondemented participants with [^{11}C]PIB negative to a certain threshold (Sheline et al., 2010). In addition, we found that Aβ deposits altered the brain regional engagement between preC/PCC and MFG/vACC even in nondemented elderly in a deposit-dependent manner.

Similarity index in DMN

The concept of a similarity index originates from recent studies regarding preC/PCC and MFG/vACC (Vogt et al., 1992; Bechara et al., 1997; Simpson et al., 2001a,b; Oshio et al., 2010). A fundamental dichotomy was reported between the functions of MFG/vACC and preC/PCC (Vogt et al., 1992), in which the preC/PCC subserves evaluative functions, such as monitoring sensory events in spatial orientation and memory (Vogt et al., 1992; Oshio et al., 2010), and the MFG/vACC subserves primarily executive functions for emotional control (Bechara et al., 1997; Simpson et al., 2001a,b). When an individual is awake and alert and yet not actively engaged in an attention-demanding task (i.e., default mode), brain activities in preC/PCC and MFG/vACC would predominate in gathering and evaluating information broadly arising in the external and internal milieu (Simpson et al., 2001a). Once focused attention is required, brain activity within these areas may be attenuated. This attenuation in activity reflects a necessary reduction in resources devoted to general information collection and evaluation. Thus, neural engagement between preC/PCC and MFG/vACC would enhance the flexible reallocation of attentional resources, which may be crucial to perform cognitive tasks. As shown in the present study, this functional coupling of medial frontoposterior DMN seems to be disrupted by Aβ deposition in DMN along with deterioration of cognitive performance.

[^{11}C]PIB accumulation in the nondemented elderly subjects

Our results confirmed that [^{11}C]PIB uptake can be a biological marker for brain functional deterioration during the preclinical state of amyloid pathology. This preclinical significance of [^{11}C]PIB uptake cannot be recognized after development of de-

mentia in previous studies. Total amyloid level did not correlate with disease progression in histologically proven AD patients (Lue et al., 1999; McLean et al., 1999), and in clinically diagnosed AD patients, there was no significant association between [^{11}C]PIB uptake and cognitive deterioration or clinical severity (Rowe et al., 2007; Yokokura et al., 2011), or only a weak association (Pike et al., 2007). This [^{11}C]PIB accumulation seemed to reach a plateau at the level of dementia with moderate clinical severity (i.e., sum of the individual ratings of CDR >5) (Grimmer et al., 2009). In addition, recent studies also showed that [^{11}C]PIB uptake affected cognitive performance in normal aging (Pike et al., 2007; Mormino et al., 2009; Rentz et al., 2010). These lines of evidence confirm that [^{11}C]PIB uptake can be used as a surrogate marker for reduced cognitive reserve during the preclinical state of amyloid pathology. In this pathology, one of the amyloid species (soluble oligomers) is considered to be a more powerful pathogen than the insoluble amyloid fibrils in AD (Montalto et al., 2007). In human studies, increased soluble Aβ levels in the AD cerebral cortices were highly correlated with disease severity (Lue et al., 1999; McLean et al., 1999). As [^{11}C]PIB cannot distinguish insoluble from soluble Aβ (Klunk et al., 2004), we do not currently know how much soluble Aβ does harm to the brain *in vivo* directly. However, the present observations may support the suggestion that soluble Aβ (oligomer) depicted partly by [^{11}C]PIB plays a central role in cognitive deterioration in the elderly. A specific probe for soluble oligomers would be desirable to gain a further understanding of its role in normal brain aging and in subjects with preclinical AD.

Hemodynamic features and glucose metabolism in DMN

In the present study, resting glucose metabolism in DMN failed to show significant correlation with hemodynamic similarity index in DMN or performance of working memory (Fig. 5*A*). However, exploratory SPM analysis of [^{18}F]FDG images showed a positive correlation between hemodynamic similarity index and glucose metabolism in the temporooccipital region (Fig. 5*B*), which is also considered part of the lateral DMN (Fox et al., 2005; Raichle and Snyder, 2007). It is generally acknowledged that low glucose metabolism in this region is likely associated with future cognitive decline in normal subjects (Jagust et al., 2006). Thus, glucose metabolism measured by [^{18}F]FDG-PET in the lateral cortex of the brain may be involved in deterioration of task-induced brain functions in aging. It was recently reported that unlike [^{18}F]FDG-based glucose metabolism reflecting anaerobic glycolysis, aerobic glycolysis in DMN is highlighted in preclinical Aβ deposition (Vlassenko et al., 2010). Indeed, our results were consistent with their suggestion because [^{18}F]FDG-SUVR reduction in preC/PCC and MFG/vACC was not significantly associated with DMN dysfunction. As the results of Vlassenko et al. (2010) were obtained by comparing different sets of groups, further studies are needed to confirm this by focusing on changes in aerobic glycolysis in DMN and brain hemodynamic discordance in the same group of nondemented elderly people. Age-related reduction of [^{18}F]FDG in the superior temporal cortex (Fig. 5) in the present study might reflect the morphological changes because [18F]FDG-SUVR of the bilateral perisylvian areas decreased with age (Yanase et al., 2005).

Conclusion

Here we show for the first time that Aβ deposition in the brain of the healthy elderly is linked to a pathophysiological mechanism of impaired neuronal connectivity in DMN and the resultant decline of working memory.

References

Bechara A, Damasio H, Tranel D, Damasio AR (1997) Deciding advantageously before knowing the advantageous strategy. Science 275:1293–1295.

Birn RM, Diamond JB, Smith MA, Bandettini PA (2006) Separating respiratory-variation-related fluctuations from neuronal-activity-related fluctuations in fMRI. Neuroimage 31:1536–1548.

Brett M, Anton JL, Valabregue R, Poline JB (2002) Region of interest analysis using an SPM toolbox [abstract]. Paper presented at the 8th International Conference on Functional Mapping of the Human Brain, Sendai, Japan.

Buckner RL, Snyder AZ, Shannon BJ, LaRossa G, Sachs R, Fotenos AF, Sheline YI, Klunk WE, Mathis CA, Morris JC, Mintun MA (2005) Molecular, structural, and functional characterization of Alzheimer's disease: evidence for a relationship between default activity, amyloid, and memory. J Neurosci 25:7709–7717.

Cabeza R, Nyberg L (2000) Imaging cognition II: an empirical review of 275 PET and fMRI studies. J Cogn Neurosci 12:1–47.

Drzezga A, Lautenschlager N, Siebner H, Riemenschneider M, Willoch F, Minoshima S, Schwaiger M, Kurz A (2003) Cerebral metabolic changes accompanying conversion of mild cognitive impairment into Alzheimer's disease: a PET follow-up study. Eur J Nucl Med Mol Imaging 30:1104–1113.

Dubois B, Slachevsky A, Litvan I, Pillon B (2000) The FAB: a Frontal Assessment Battery at bedside. Neurology 55:1621–1626.

Fox MD, Snyder AZ, Vincent JL, Corbetta M, Van Essen DC, Raichle ME (2005) The human brain is intrinsically organized into dynamic, anticorrelated functional networks. Proc Natl Acad Sci U S A 102:9673–9678.

Fratiglioni L, Launer LJ, Andersen K, Breteler MM, Copeland JR, Dartigues JF, Lobo A, Martinez-Lage J, Soininen H, Hofman A (2000) Incidence of dementia and major subtypes in Europe: a collaborative study of population-based cohorts. Neurologic Diseases in the Elderly Research Group. Neurology 54:S10–S15.

Greicius MD, Krasnow B, Reiss AL, Menon V (2003) Functional connectivity in the resting brain: a network analysis of the default mode hypothesis. Proc Natl Acad Sci U S A 100:253–258.

Greicius MD, Srivastava G, Reiss AL, Menon V (2004) Default-mode network activity distinguishes Alzheimer's disease from healthy aging: evidence from functional MRI. Proc Natl Acad Sci U S A 101:4637–4642.

Grimmer T, Henriksen G, Wester HJ, Förstl H, Klunk WE, Mathis CA, Kurz A, Drzezga A (2009) Clinical severity of Alzheimer's disease is associated with PIB uptake in PET. Neurobiol Aging 30:1902–1909.

Gusnard DA, Raichle ME (2001) Searching for a baseline: functional imaging and the resting human brain. Nat Rev Neurosci 2:685–694.

Hampson M, Driesen NR, Skudlarski P, Gore JC, Constable RT (2006) Brain connectivity related to working memory performance. J Neurosci 26:13338–13343.

Hedden T, Van Dijk KR, Becker JA, Mehta A, Sperling RA, Johnson KA, Buckner RL (2009) Disruption of functional connectivity in clinically normal older adults harboring amyloid burden. J Neurosci 29:12686–12694.

Herscovitch P, Markham J, Raichle ME (1983) Brain blood flow measured with intravenous H2(15)O. I. Theory and error analysis. J Nucl Med 24:782–789.

Jagust W, Gitcho A, Sun F, Kuczynski B, Mungas D, Haan M (2006) Brain imaging evidence of preclinical Alzheimer's disease in normal aging. Ann Neurol 59:673–681.

Jorm AF, Jolley D (1998) The incidence of dementia: a meta-analysis. Neurology 51:728–733.

Klunk WE, Engler H, Nordberg A, Wang Y, Blomqvist G, Holt DP, Bergström M, Savitcheva I, Huang GF, Estrada S, Ausén B, Debnath ML, Barletta J, Price JC, Sandell J, Lopresti BJ, Wall A, Koivisto P, Antoni G, Mathis CA, et al. (2004) Imaging brain amyloid in Alzheimer's disease with Pittsburgh Compound-B. Ann Neurol 55:306–319.

Lowe MJ, Mock BJ, Sorenson JA (1998) Functional connectivity in single and multislice echoplanar imaging using resting-state fluctuations. Neuroimage 7:119–132.

Lue LF, Kuo YM, Roher AE, Brachova L, Shen Y, Sue L, Beach T, Kurth JH, Rydel RE, Rogers J (1999) Soluble amyloid beta peptide concentration as a predictor of synaptic change in Alzheimer's disease. Am J Pathol 155:853–862.